Research article

How many sirtuin genes are out there? evolution of sirtuin genes in vertebrates with a description of a new family member

Juan C. Opazo[1,2,3], Michael W. Vandewege[4], Federico G. Hoffmann[5,6], Kattina Zavala[2], Catalina Meléndez[7], Charlotte Luchsinger[8], Viviana A. Cavieres[7], Luis Vargas-Chacoff[1,9,10,11], Francisco J. Morera[1,12], Patricia V. Burgos[7,13,14], Cheril Tapia-Rojas[7,13], Gonzalo A. Mardones[1,8,15]

[1]Integrative Biology Group, Universidad Austral de Chile, Valdivia, Chile.
[2]Instituto de Ciencias Ambientales y Evolutivas, Facultad de Ciencias, Universidad Austral de Chile, Valdivia, Chile.
[3]Millennium Nucleus of Ion Channel-Associated Diseases (MiNICAD), Valdivia, Chile.
[4]Department of Biology, Eastern New Mexico University, Portales, New Mexico, USA.
[5]Department of Biochemistry, Molecular Biology, Entomology, and Plant Pathology, Mississippi State University, Starkville, Mississippi, USA.
[6]Institute for Genomics, Biocomputing and Biotechnology, Mississippi State University, Starkville, Mississippi, USA.
[7]Centro de Biología Celular y Biomedicina (CEBICEM), Facultad de Medicina y Ciencia, Universidad San Sebastián, Santiago, Chile.
[8]Department of Physiology, School of Medicine, Universidad Austral de Chile, Valdivia, Chile.
[9]Instituto de Ciencias Marinas y Limnológicas, Universidad Austral de Chile, Valdivia, Chile.
[10]Centro Fondap de Investigación de Altas Latitudes (IDEAL), Universidad Austral de Chile, Valdivia, Chile.
[11]Millennium Institute Biodiversity of Antarctic and Subantarctic Ecosystems, BASE, Universidad Austral de Chile, Valdivia, Chile.
[12]Applied Biochemistry Laboratory, Facultad de Ciencias Veterinarias, Instituto de Farmacología y Morfofisiología, Universidad Austral de Chile, Valdivia, Chile.
[13]Centro Ciencia & Vida, Fundación Ciencia & Vida, Santiago, Chile.
[14]Centro de Envejecimiento y Regeneración (CARE-UC), Facultad de Ciencias Biológicas, Pontificia Universidad Católica, Santiago, Chile.
[15]Center for Interdisciplinary Studies of the Nervous System (CISNe), Universidad Austral de Chile, Valdivia, Chile.

Corresponding authors:
Juan C. Opazo, jopazo@gmail.com
Gonzalo A. Mardones, gonzalo.mardones@uach.cl

Abstract

Studying the evolutionary history of gene families is a challenging and exciting task with a wide range of implications. In addition to exploring fundamental questions about the origin and evolution of genes, disentangling their evolution is also critical to those who do functional/structural studies to allow a deeper and more precise interpretation of their results in an evolutionary context. The sirtuin gene family is a group of genes that are involved in a variety of biological functions mostly related to aging. Their duplicative history is an open question, as well as the definition of the repertoire of sirtuin genes among vertebrates. Our results show a well-resolved phylogeny that represents an improvement in our understanding of the duplicative history of the sirtuin gene family. We identified a new sirtuin family member (SIRT3-like) that was apparently lost in the last common ancestor of amniotes, but retained in all other groups of jawed vertebrates. According to our experimental analyses, elephant shark SIRT3-like protein is located in mitochondria, the overexpression of which leads to an increase in cellular levels of ATP. Moreover, *in vitro* analysis demonstrated it has deacetylase activity being modulated in a similar way to mammalian SIRT3. Our results indicate that there are at least eight sirtuin paralogs among vertebrates and that all of them can be traced back to the last common ancestor of the group that existed between 676 and 615 millions of years ago.

Keywords: aging, deacetylase, gene family evolution, gene duplication, mitochondria, SIRT.

Introduction

The availability of whole-genome sequences in species of all main groups of vertebrates represents an opportunity to unravel the evolution of gene families. The number of genomes and their phylogenetic representativeness in the vertebrate tree of life allows performing robust inferences regarding how gene family members are related to each other and their modes of evolution (Nei and Rooney 2005). The available genomes also open an opportunity to discover new gene lineages that are not currently described maybe because they are not present in model species and/or to the absence of appropriate evolutionary analyses (Wichmann et al. 2016; Céspedes et al. 2017; Himmel et al. 2020). Gene copy number variation could be seen as a natural experiment (Albertson et al. 2009) that could help understand the evolutionary fate of duplicated genes, as individuals with different repertoires can, in principle, fulfill the biological functions with a different combination of paralogs.

The sirtuin gene family, class III of histone deacetylase enzymes (HDACs), is an ancient group of genes that, in mammals, is composed of seven paralogs (SIRT1-7) grouped into four classes (Fig. 1)(Frye 2000; Frye 2006). Sirtuin genes are involved in a variety of biological functions mostly related to aging, metabolic regulation, stress response, cell cycle among others (Fig. 1) (Michan and Sinclair 2007; Greiss and Gartner 2009; Haigis and Sinclair 2010; Zhao et al. 2019; Zhang et al. 2020). All sirtuin genes have a conserved catalytic domain and variable carboxy- and amino terminal domains. Most family members possess deacetylase activity, while others have, in addition to weak deacetylase activity, other enzymatic activities like ADP-ribosyltransferase, desuccinylase and demalonylase (Fig. 1). Further, they are located in different subcellular compartments and associated to different biological functions (Fig. 1).

The evolution of the sirtuin genes is an open question. There are multiple phylogenetic hypotheses describing evolutionary relationships among the paralogs in the sirtuin gene family (Frye 2000; North and Verdin 2004; Frye 2006; Greiss and Gartner 2009; Pereira et al. 2011; Slade et al. 2011; Vassilopoulos et al. 2011; Costantini et al. 2013; Scholte et al. 2017; Simó-Mirabet et al. 2017; Yang et al. 2017; Rajabi et al. 2018; Kabiljo et al. 2019; Zhao et al. 2019). Differences in the taxonomic sampling, number of paralogs included, and the inclusion of outgroups, are likely contributors to this variation.

Additionally, studies that are focused on resolving evolutionary relationships are scarce, and in fact, most phylogenetic analyses for sirtuin genes are part of studies where the sirtuin duplicative history is a secondary goal. Additionally, and probably for similar reasons, there are no systematic efforts to characterize the full complement of sirtuin genes among vertebrates. Thus, unraveling the evolutionary history of sirtuin genes represents a challenging and exciting task with a wide range of implications. Because of their role in the aging process, these genes are of great interest. In addition to exploring fundamental questions about the origin and evolution of sirtuin genes, disentangling their evolution is also critical to understanding the diversification of functional and structural phenotypes present in the sirtuin gene family.

This study aims to take advantage of the genomic data available in public databases to advance our understanding of the diversity of vertebrate sirtuin genes and to infer its duplicative history. We also aim to characterize the subcellular localization, enzymatic activity, and mitochondrial activity of the newly discovered SIRT3-like gene lineage in the elephant shark (*Callorhinchus milii*) as a representative species. Our phylogenetic tree is in general well resolved, recovering sirtuin genes into two clades: 1) SIRT4, SIRT5, SIRT6 and SIRT7, and 2) SIRT1, SIRT2, SIRT3, and SIRT3-like. The new sirtuin family member (SIRT3-like) is retained in all vertebrates other than amniotes (the group that includes mammals, birds, and reptiles). Based on how sirtuin genes are related to each other and the information is already known for the other sirtuin family members, we can predict that SIRT3-like belongs to the class I, has a deacetylase activity, and is mainly located on mitochondria. Our experimental analyses confirmed our evolutionary guided inferences.

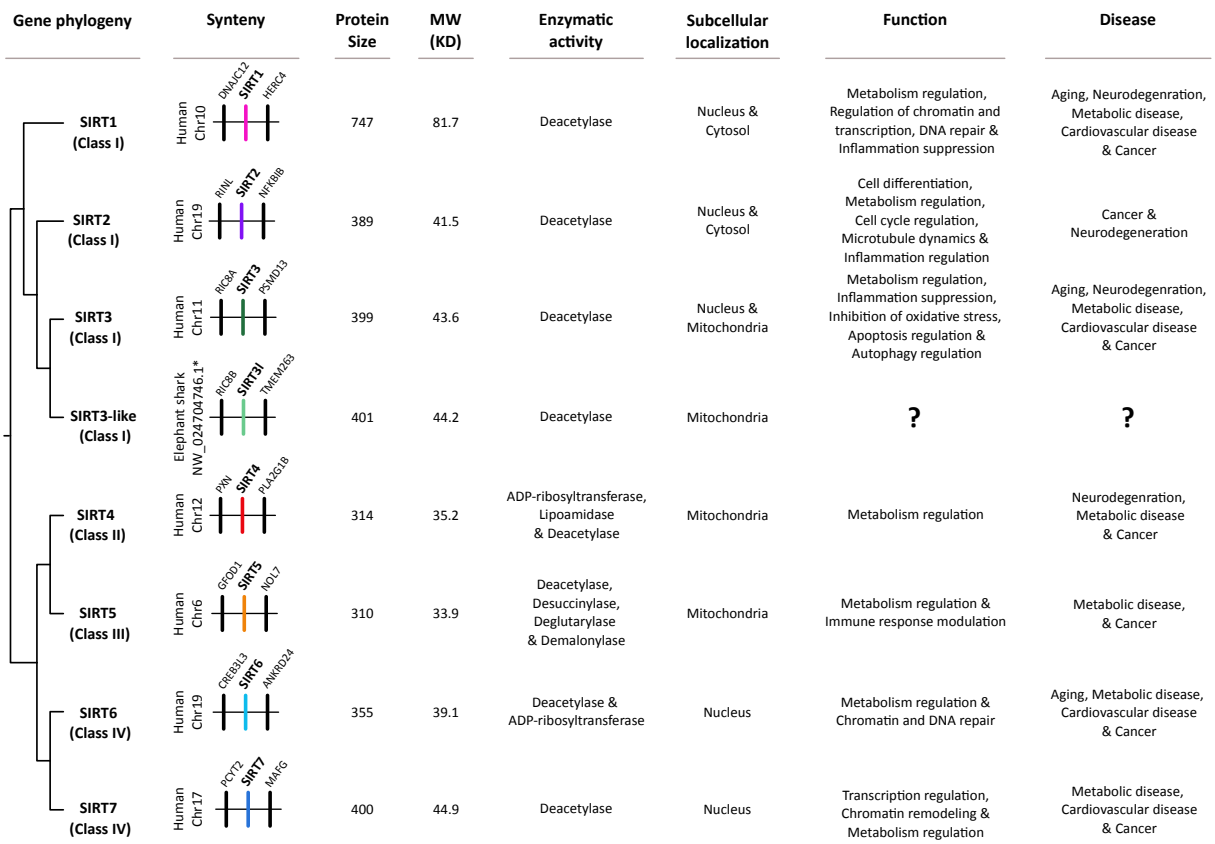

Figure 1. Gene phylogeny, synteny, protein size, molecular weight, enzymatic activity, subcellular localization, functions and diseases associated with sirtuin genes. Information regarding the sister group relationships among sirtuin genes was obtained from this study, synteny from ENSEMBL v.106 (Howe et al. 2021), protein size from Fujita and Yamashita (2018)(Fujita and Yamashita 2018), molecular weight from Vassilopoulos et al. (2011)(Vassilopoulos et al. 2011) while enzymatic activity, subcellular localization, functions and diseases from Zhang et al. (2020)(Zhang et al. 2020). In the case of the SIRT3-like of the elephant shark, synteny information was obtained from the National Center for Biotechnology Information (NCBI) (Sharma et al. 2019), protein size, molecular weight, enzymatic activity and subcellular localization from this study.

Results and Discussion

Sirtuin paralogs are recovered into two main clades

We recovered the monophyly of all sirtuin family members with strong support (Fig. 2), except for the SIRT3 clade which received moderate support (Fig. 3). In this case, the phylogenetic position of the sea lamprey (*Petromyzon marinus*) could be considered ambiguous (Fig. 3). This situation could be explained by the sequence itself, instead of the well-known compositional bias of the cyclostome genomes (Qiu et al. 2011; Kuraku

138 2013; Smith et al. 2013), given that the phylogenetic position of the other SIRT3
139 cyclostome sequence (inshore hagfish, *Eptatretus burgeri*) was recovered, as expected,
140 sister to all other vertebrate SIRT3 with strong support (Fig. 3). Additionally, our
141 phylogenetic reconstructions did not have difficulties inferring orthology for all other
142 cyclostome sirtuin genes. Further, in support of our tree topology, the sea lamprey
143 chromosomal region that harbors SIRT3 shares one syntenic gene, Bet1 Golgi vesicular
144 membrane trafficking protein-like (Bet1l), with humans.

145 According to our results, the diversity of sirtuin genes was arranged into two main
146 clades (Fig. 2). The first includes the SIRT4, SIRT5, SIRT6 and SIRT7, whereas the
147 second includes the SIRT1, SIRT2, SIRT3 and SIRT3-like lineages (Fig. 2). In the
148 literature, a diversity of phylogenetic arrangements have been proposed (Frye 2000;
149 North and Verdin 2004; Frye 2006; Greiss and Gartner 2009; Hirschey 2011; Pereira et
150 al. 2011; Slade et al. 2011; Vassilopoulos et al. 2011; Costantini et al. 2013; Scholte et
151 al. 2017; Simó-Mirabet et al. 2017; Yang et al. 2017; Rajabi et al. 2018; Kabiljo et al.
152 2019; Zhao et al. 2019), not being directly comparable as different studies implemented
153 different taxonomic samplings and not all of them include outgroups. One of the above
154 mentioned studies recovered the diversity of sirtuin genes into two main clades
155 (Vassilopoulos et al. 2011), however they did not recover the sister group relationship
156 between SIRT4 and SIRT5.

157 In the first clade we recovered the sister group relationships between SIRT4 and
158 SIRT5 with strong support (Fig. 2). Evolutionary relationships between these two family
159 members are still a matter of debate, as a variety of phylogenetic positions have been
160 suggested for them (Slade et al. 2011; Vassilopoulos et al. 2011; Costantini et al. 2013;
161 Yang et al. 2017; Rajabi et al. 2018), and only in a fraction of the studies their sister group
162 relationship is supported (Frye 2000; North and Verdin 2004; Frye 2006; Greiss and
163 Gartner 2009; Hirschey 2011; Pereira et al. 2011; Scholte et al. 2017; Simó-Mirabet et al.
164 2017; Kabiljo et al. 2019; Zhao et al. 2019). In the same clade, we also recovered SIRT6
165 sister to the clade containing SIRT7 sequences with strong support (Fig. 2). The sister
166 group relationship between SIRT6 and SIRT7 has been recovered in all examined studies
167 (Frye 2000; North and Verdin 2004; Frye 2006; Greiss and Gartner 2009; Hirschey 2011;
168 Pereira et al. 2011; Scholte et al. 2017; Simó-Mirabet et al. 2017; Kabiljo et al. 2019; Zhao

169 et al. 2019), suggesting a robust support for the sister group relationship between these
170 sirtuin lineages. The sister-group relationship between the SIRT6/SIRT7 and
171 SIRT4/SIRT5 clades is moderately supported (Fig. 2), being consistent with the diversity
172 of topologies reported in the literature, and suggesting that more work is necessary (Frye
173 2000; North and Verdin 2004; Frye 2006; Greiss and Gartner 2009; Hirschey 2011; Slade
174 et al. 2011; Vassilopoulos et al. 2011; Costantini et al. 2013; Scholte et al. 2017; Simó-
175 Mirabet et al. 2017; Yang et al. 2017; Rajabi et al. 2018; Kabiljo et al. 2019; Zhao et al.
176 2019). In the second clade, there is a broad consensus in the literature that SIRT2 shares
177 a common ancestor more recently in time with SIRT3 than with any other sirtuin family
178 member, and that the clade containing SIRT1 sequences is sister to the SIRT2/SIRT3
179 clade (Frye 2000; North and Verdin 2004; Frye 2006; Greiss and Gartner 2009; Hirschey
180 2011; Pereira et al. 2011; Slade et al. 2011; Vassilopoulos et al. 2011; Costantini et al.
181 2013; Scholte et al. 2017; Simó-Mirabet et al. 2017; Yang et al. 2017; Rajabi et al. 2018;
182 Zhao et al. 2019). Accordingly, we recovered the same evolutionary relationships with
183 strong support (Fig. 2).
184 In summary, we present a phylogenetic analysis based on a taxonomic sampling
185 that included representative species from all main groups of vertebrates for all sirtuin
186 family members. Our phylogenetic tree is in general well resolved (Fig. 2), representing
187 an advance in our understanding of the duplicative history of the sirtuin gene family. In
188 comparison to the gene trees currently available in the literature our tree topology
189 represents a new hypothesis for their duplicative history.
190

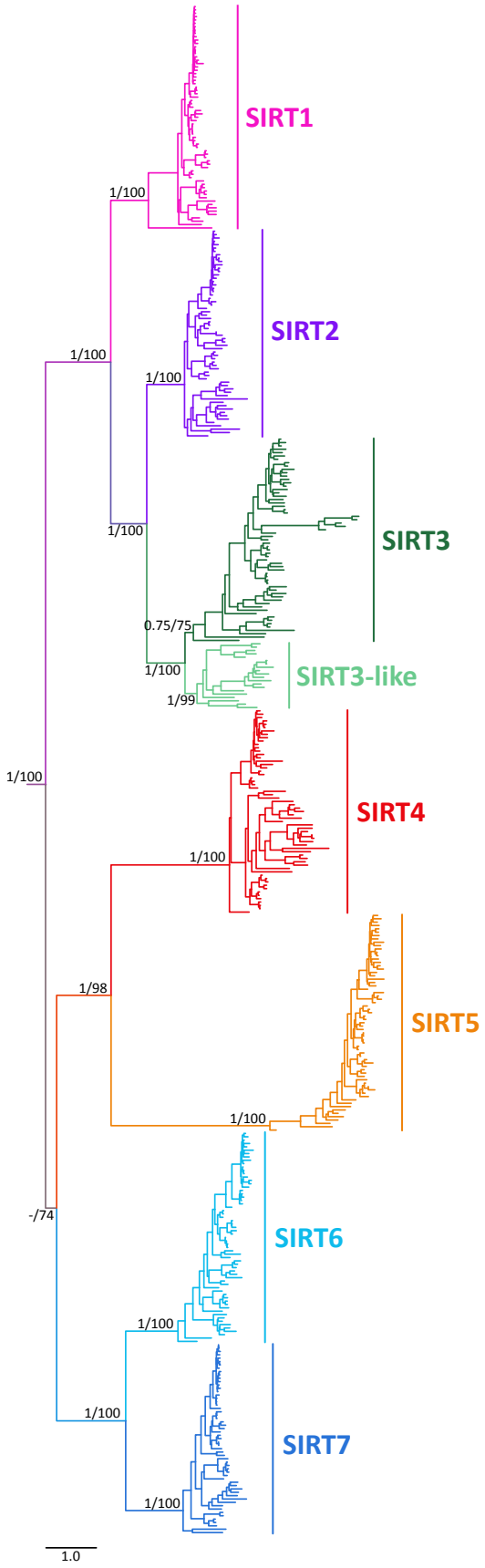
SIRT1
SIRT2
SIRT3
SIRT3-like
SIRT4
SIRT5
SIRT6
SIRT7
1/100
1/100
1/100
1/100
0.75/75
1/100
1/99
1/100
1/100
1/98
1/100
-/74
1/100
1/100
1/100
1.0

191

192 **Figure 2.** Maximum likelihood tree showing sister group relationships among sirtuin
193 genes of vertebrates. Numbers on the nodes correspond to support from the aBayes and
194 ultrafast bootstrap values. Nicotinamide Nucleotide Transhydrogenase (NNT) sequences
195 from the human (*Homo sapiens*) mouse (*Mus musculus*), spotted gar (*Lepisosteus*
196 *oculatus*) and zebrafish (*Danio rerio*) were used as outgroups (not shown). The scale
197 denotes substitutions per site and colors represent sirtuin lineages.
198

199 Identification of a new sirtuin gene family member, SIRT3-like

200 In our analyses, we identified a new sirtuin family member (Fig. 2 and 3), SIRT3-like,
201 which is present in a fraction of the vertebrate tree of life (Fig. 4) that was recovered sister
202 to the SIRT3 clade with strong support (Fig. 2 and 3). Synteny conservation provides
203 further support to the monophyly of the SIRT3-like gene lineage in gnathostomes (Fig.
204 5a), as genes found at the 5` side (POLR3B, RFX4 and RIC8B) and 3` side (TMEM263,
205 MTERF2, and CRY1) of the SIRT3-like gene are well conserved (Fig. 5a). Synteny is also
206 conserved in species in which the SIRT3-like gene was lost (Fig. 5a). Among vertebrates,
207 we found orthologs of the SIRT3-like gene in representative species of cartilaginous fish,
208 bony fish, coelacanth, and amphibians (Fig. 4). A comparison of the genomic region of
209 the tropical clawed frog (*Xenopus tropicalis*), which possesses the SIRT3-like gene, with
210 the corresponding region in the human (*Homo sapiens*), opossum (*Monodelphis*
211 *domestica*), chicken (*Gallus gallus*), gharial (*Gavialis gangeticus*), red-eared slider
212 (*Trachemys scripta*) and green anole (*Anolis carolinensis*) strongly suggests that the
213 SIRT3-like gene is not present in the vertebrate lineages that these species represent
214 (Fig. 5b). The absence of the SIRT3-like gene in mammals, birds and reptiles indicates
215 that it was probably lost in the common ancestor of the group, between 352 and 312
216 millions of years ago (Kumar et al. 2017). In the case of cyclostomes, we found in the sea
217 lamprey (*Petromyzon marinus*) a chromosomal region (Chr3) that possess TMEM263 and
218 POLR3B separated by 44 base pairs, suggesting that all the genes that should be in
219 between (RFX4, RIC8B, SIRT3-like) were lost in cyclostomes. Alternatively, it is possible
220 that SIRT3-like, and all the other genes are present in cyclostome genomes, but not in
221 the current genome assembly. In the past, Pereira et al. (2011), with a limited taxonomic
222 sampling, identified a clade sister to a group containing SIRT3 sequences. This gene
223 lineage included sequences from three species with an evolutionary history of whole-
224 genome duplications, two teleost fish (zebrafish, *Danio rerio*, and green spotted puffer,

225 *Tetraodon nigroviridis*), and one amphibian (African clawed frog, *Xenopus laevis*),
226 complicating the definition of their duplicative history. Thus, our results, including a
227 balanced taxonomic sampling of all main vertebrate groups and appropriate phylogenetic
228 searches, define the existence of the SIRT3-like gene lineage and its phyletic distribution.

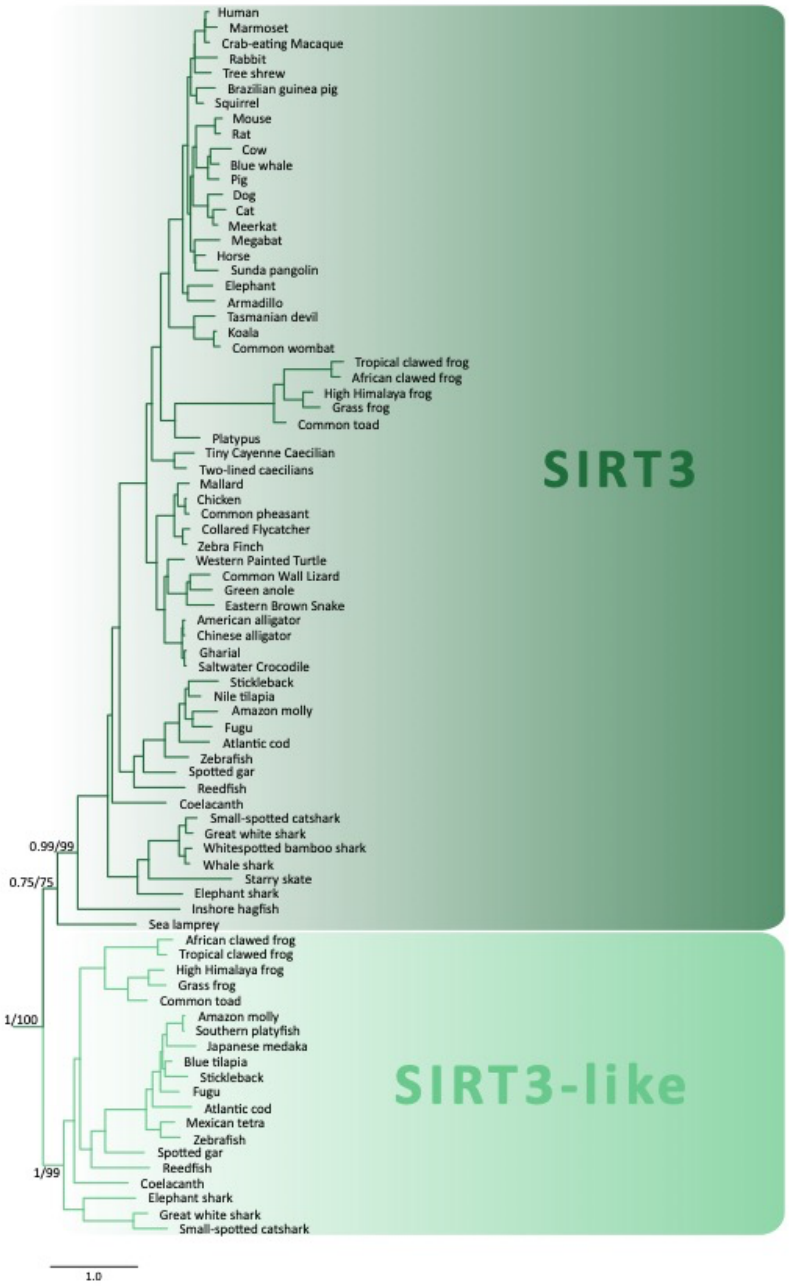

229

230 **Figure 3.** Maximum likelihood tree showing sister group relationships among SIRT3 and
231 SIRT3-like genes in vertebrates. Numbers on the nodes correspond to support from the
232 aBayes and ultrafast bootstrap values. The scale denotes substitutions per site and colors
233 represent gene lineages. This tree does not represent a novel phylogenetic analysis, it is

the SIRT3/SIRT3-like clade that was recovered from figure 2. The scale denotes substitutions per site and colors represent sirtuin lineages.

The lack of the SIRT3-like gene can be interpreted in different ways. We can think that the loss of SIRT3-like could have no physiological impact if the functional role of the lost gene is assumed by other family members, consistent with the idea that gene families possess functional redundancy (Ohno 1985; Félix and Barkoulas 2015; Albalat and Cañestro 2016). Alternatively, we can also think of gene loss as a source of adaptive evolution (Olson 1999; Albalat and Cañestro 2016; Helsen et al. 2020). The description of new gene lineages is not uncommon in the literature (Wichmann et al. 2016; Himmel et al. 2020; Opazo et al. 2021). It could be mainly attributed to the presence in non-model species and/or the absence of proper evolutionary analyses. The existence of species with different gene repertoires is an opportunity to better understand the evolutionary fate of duplicated genes (Lynch and Conery 2000) and the biological functions associated to a group of genes.

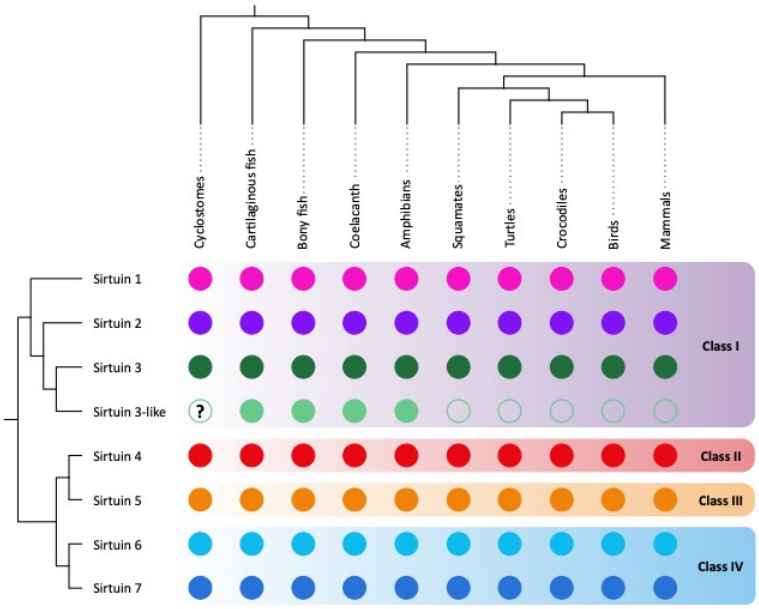

Figure 4. Phyletic distribution of sirtuin genes in vertebrates. The sister group relationships among sirtuin genes was obtained from this study, whereas, organismal phylogeny was obtained from the most updated phylogenetic hypotheses available in the literature (Iwabe et al. 2005; Delsuc et al. 2006; Delsuc et al. 2008; Hara et al. 2018). The

colors of the circles are those used in figure 2 to define sirtuin gene lineages, whereas the classes to which the different sirtuins belong are shown with shading. The question mark denotes that we cannot determine whether or not the sirtuin3-like gene is present in cyclostomes.

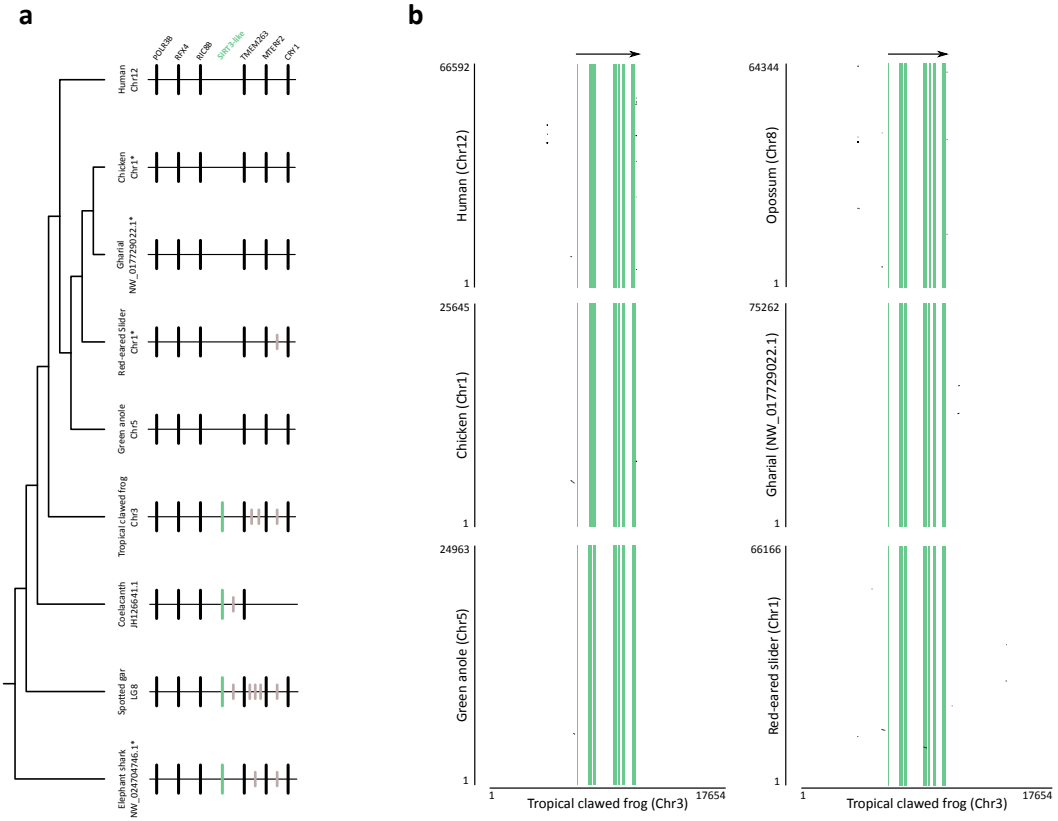

Figure 5. a Patterns of conserved synteny in the chromosomal region that harbor SIRT3-like genes in gnathostomes. Asterisks denote that the orientation of the genomic piece is from 3´ to 5´, gray lines represent intervening genes that do not contribute to conserved synteny. **b** Pairwise dot-plot comparison of the genomic region of the tropical clawed frog (*Xenopus tropicalis*) with the corresponding region in the human (*Homo sapiens*), opossum (*Monodelphis domestica*), chicken (*Gallus gallus*), gharial (*Gavialis gangeticus*), red-eared slider (*Trachemys scripta*) and green anole (*Anolis carolinensis*). Light green vertical lines denote exons and regions in between are introns. Dot plots were based on the complete coding region in addition to 6.7 kb of upstream and downstream flanking sequence.

An amino acid alignment of the SIRT3-like and SIRT3 sequences shows that the catalytic domain of SIRT3-like is well conserved, where six amino acid positions were

identified as diagnostic characters (Fig. 6). The amino acid divergence of the SIRT3-like catalytic domain varies from 32.2% (spotted gar vs coelacanth) to 33.6% (spotted gar vs elephant shark). The same comparisons for the SIRT3 catalytic domain show slightly lower amino acid divergence values, between 24.8% (spotted gar vs coelacanth) and 31.0% (coelacanth vs elephant shark). As expected, the interparalog distance (SIRT3 vs SIRT3-like) of the catalytic domains shows higher divergence values, ranging from 40.7% (spotted gar SIRT3 vs spotted gar SIRT3-like) and 43.6% (elephant shark SIRT3 vs elephant shark SIRT3-like). Although nothing is known about the protein encoded by the SIRT3-like gene, based on how sirtuin genes are evolutionarily related and the information already known for the other family members (Fig. 1), we can speculate that SIRT3-like belongs to the class I, is mainly located on the mitochondria/nucleus, and has deacetylase activity. From a functional perspective it should perform functions similar to what has been described for SIRT3 (Fig. 1) (Brown et al. 2013; McDonnell et al. 2015; Zhang et al. 2020). It is important to highlight that the inferences regarding a newly discovered gene are better performed if they are phylogenetically guided.

Figure 6. Alignment of the catalytic domain of SIRT3 in humans (*Homo sapiens*), and SIRT3 and SIRT3-like of spotted gar (*Lepisosteus oculatus*), coelacanth (*Latimeria chalumnae*) and elephant shark (*Callorhinchus milii*). The shaded region denotes the catalytic domain. Diagnostic characters -i.e. amino acids positions that distinguish

between SIRT3 and SIRT3-like gene lineages - are indicated with a rectangle and green colors.

Expression pattern of sirtuin gene family members

Our next step in characterizing the SIRT3-like gene was to investigate whether it is transcribed and if it was, to characterize the transcription pattern. To do this, we mapped RNASeq reads to reference gene sequences of representative species of vertebrates and examined transcript abundance. In agreement with the transcription pattern reported for sirtuin genes (Stelzer et al. 2016; Kabiljo et al. 2019), our results show that although they exhibited wide variance in tissue expression, sirtuin genes are expressed in almost all tissues, including the novel SIRT3-like gene lineage (Fig. 7). In the case of the tropical clawed frog, the SIRT3-like gene is transcribed at a similar level in all tissues, other than the ovary where high transcription levels were estimated (Fig. 7). Coincident with the pattern observed in the tropical clawed frog, the elephant shark SIRT3-like gene is mostly transcribed in the ovary (Fig. 7). In the case of the zebrafish, although our transcription level estimations did not follow the trend previously mentioned, an extensive study examining the expression of all sirtuin genes in zebrafish showed that the SIRT3-like gene in this species is mainly expressed in the ovary (Pereira et al. 2011). Thus, in addition to showing that the SIRT3-like gene is transcribed, our analyses allow us to suggest that this gene could be involved in biological processes associated with reproduction. This observation seems not to be unexpected as for SIRT3 there are many studies in which its functions related to reproduction have been reported (Zhao et al. 2016; Tatone et al. 2018; Vazquez et al. 2020; Di Emidio et al. 2021).

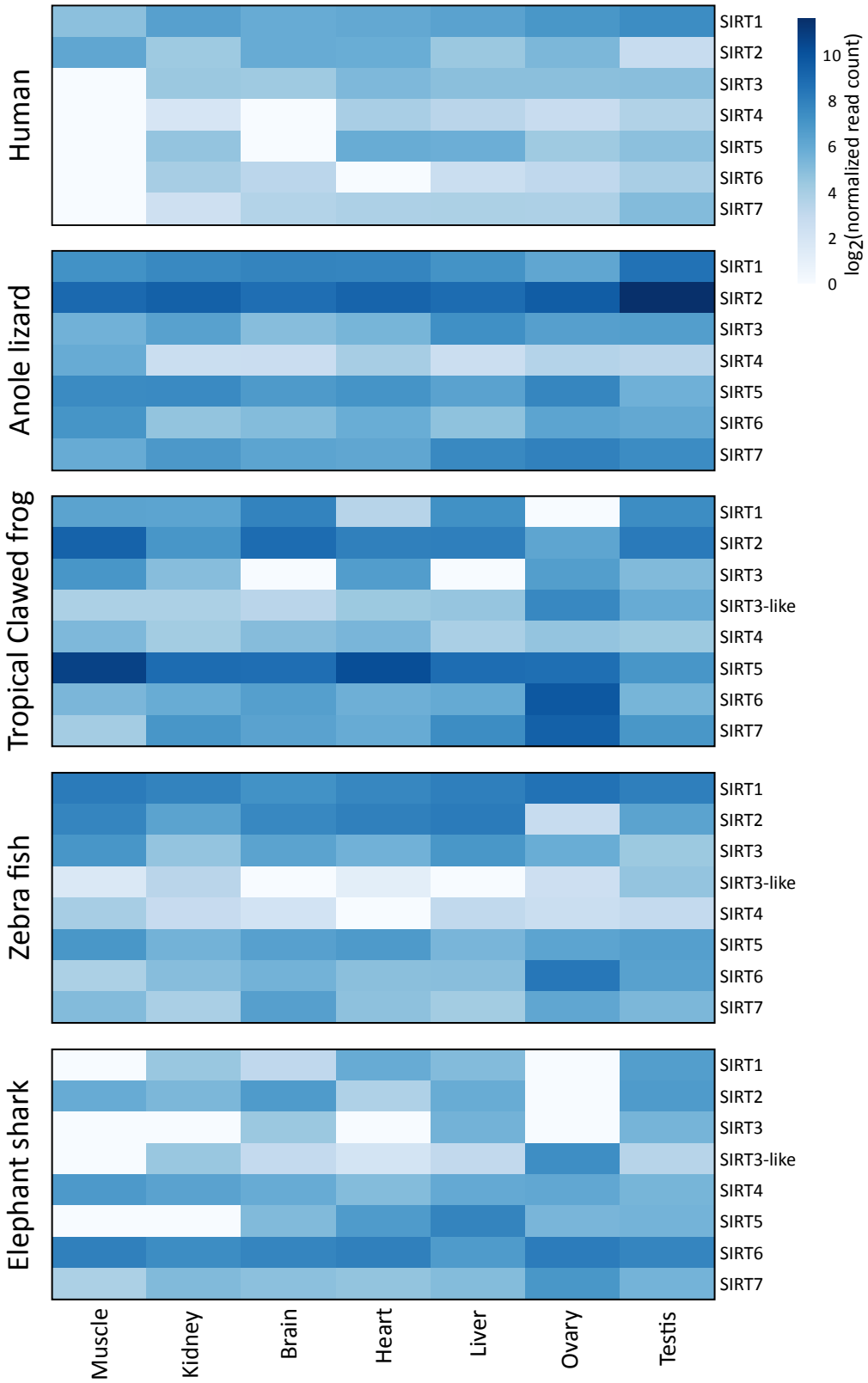
Human
Anole lizard
Tropical Clawed frog
Zebra fish
Elephant shark
SIRT1
SIRT2
SIRT3
SIRT3-like
SIRT4
SIRT5
SIRT6
SIRT7
Muscle
Kidney
Brain
Heart
Liver
Ovary
Testis
log2(normalized read count)
0
2
4
6
8
10

322

323 **Figure 7.** Heatmap representation of transcription levels of sirtuin genes among
324 vertebrates. Transcription values were calculated independently for each species and
325 normalized over all tissues.
326

327 Elephant shark SIRT3-like protein localizes to mitochondria

328 To further explore the structural relationship between SIRT3 and SIRT3-like proteins, we
329 performed an unbiased protein structure homology modeling of SIRT3-like proteins from
330 elephant shark (*Callorhinchus milii*), spotted gar (*Lepisosteus oculatus*), salmon (*Salmo*
331 *salar*) and coelacanth (*Latimeria chalumnae*). Models of SIRT3-like proteins were
332 generated by the SWISS-MODEL workspace that used as template crystal structure
333 models of human SIRT3: 4bvh.1.A for elephant shark, 5z94.1.A for spotted gar, 5d7n.3.A
334 for salmon and 5bwo.1.B for coelacanth (data not shown). All models generated comprise
335 only the central portion of the SIRT3-like proteins where the catalytic and its regulatory
336 regions are expected to be. The overall root mean square deviation for 272
337 superimposable Cα coordinates for the models of human SIRT3 (pdb: 4bvh.1.A; amino
338 acids G121 to G392) and elephant shark SIRT3-like (amino acids G95 to Q365) is 0.101
339 Å (Fig. 8a), suggesting extensive structural match. SIRT proteins possess evolutionary
340 conserved, distinct cellular localizations and functions (Fig. 1). Some sirtuins localize in
341 more than one compartment, like SIRT1 and SIRT2 that localize to the nucleus and
342 cytosol, and SIRT3 that localizes mainly to the mitochondrial matrix, but with a small
343 fraction localizing to the nucleus (Scher et al. 2007). In contrast, SIRT4 and SIRT5 localize
344 only to mitochondria, and SIRT6 and SIRT7 localize only to the nucleus. The sequence
345 and structural comparison between SIRT3-like and SIRT3 proteins, as well as subcellular
346 localization prediction by LocTree3 (Goldberg et al. 2014), suggest that the localization
347 of SIRT3-like proteins is also in the mitochondria. To determine the subcellular
348 localization of SIRT3-like proteins, we chose to analyze SIRT3-like from elephant shark.
349 To this end, we expressed in human cultured cells full-length elephant shark SIRT3-like
350 tagged with three copies of the c-Myc epitope at the C-terminus (SIRT3-like-3myc). To
351 obtain biochemical evidence of the expression of this protein, we performed immunoblot
352 analysis with monoclonal antibody 9E10 against the c-Myc epitope, which showed the

353 detection of an expected 48.3 kDa protein in all cell lines analyzed (Fig. 8b). Fluorescence
354 microscopy analysis of human H4 neuroglioma cells expressing SIRT3-like-3myc showed
355 decoration by the anti-c-Myc antibody of structures highly reminiscent of mitochondria, in
356 addition to a faint fluorescent signal in the rest of the cytoplasm (Fig. 8c, d). Mitochondria
357 localization of SIRT3-like-3myc was confirmed by co-localization with the fluorescent
358 signal of MitoTracker Orange (Fig. 8c). Importantly, SIRT3-like-3myc showed no
359 localization in any other major compartment, as shown by lack of localization in the
360 nucleus (detected with the nuclear stain DAPI; Fig. 8c, d), the Golgi apparatus (detected
361 with antibody against TGN46; Fig. 8c, d), or the endoplasmic reticulum (detected with
362 antibody against P63; Fig. 8d). The same pattern of expression of SIRT3-like-3myc was
363 obtained using other human cell lines, such as HeLa or MDA-MB-231 cells (data not
364 shown). Altogether, these results indicate that SIRT3-like proteins are targeted to the
365 mitochondria.

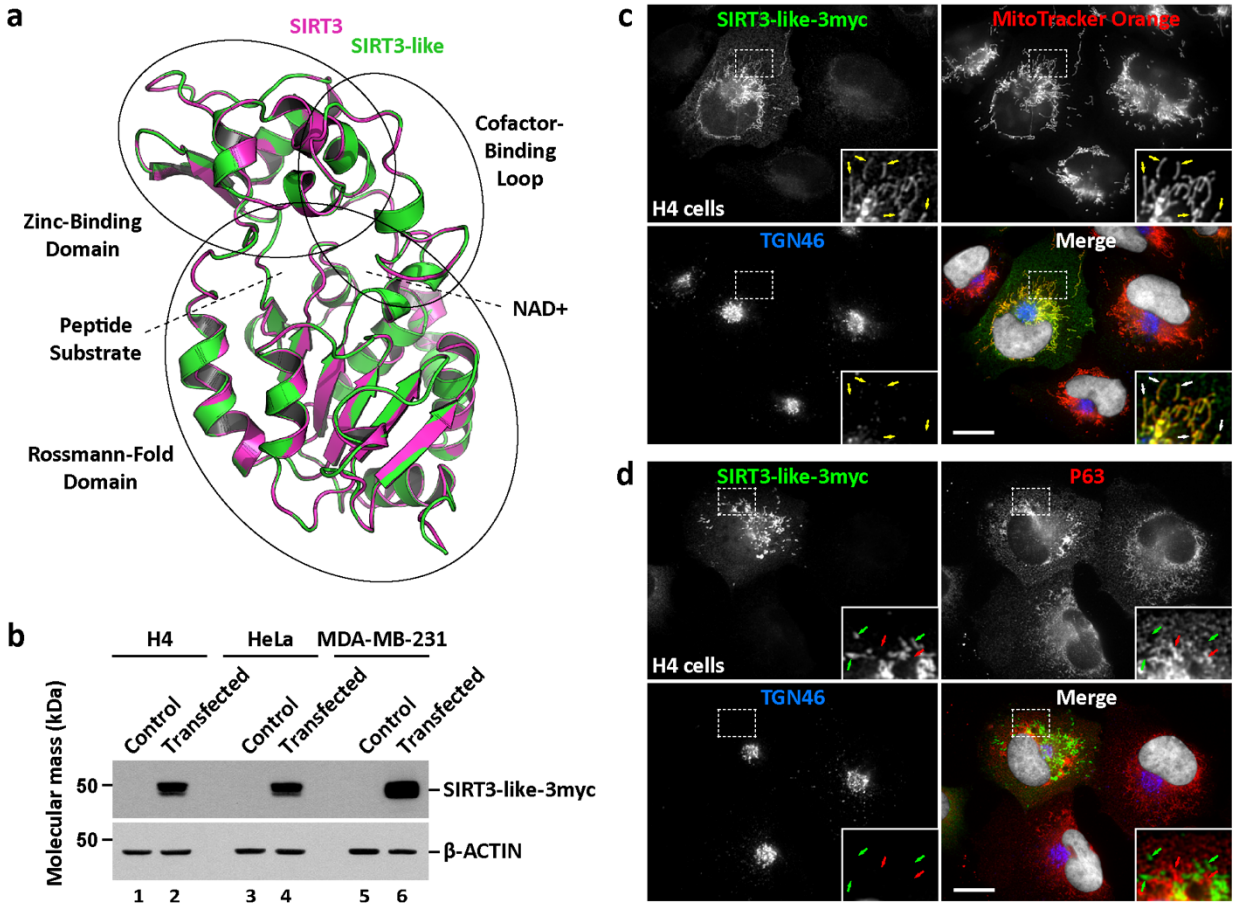

366
367

368 **Figure 8.** Structural model of elephant shark SIRT3-like and expression in mammalian
369 cells of SIRT3-like-3myc. **a** Superposition of the ribbon representations of elephant shark
370 SIRT3-like (green model; amino acids G95 to Q365) and human SIRT3 (magenta model;
371 pdb: 4bvh.1.A; amino acids G121 to G392). Depicted in ellipses are the indicated
372 functional/structural domains of SIRT3 and in dotted lines the binding sites for peptide
373 substrates and NAD^+. **b** The indicated cells were left untreated (Control, lanes 1, 3 and
374 5) or transfected to express SIRT3-like-3myc (lanes 2, 4 and 6), followed by immunoblot
375 analysis with antibody against the c-Myc epitope or antibody against β-ACTIN used as
376 loading control. The position of molecular mass markers is indicated on the left. SIRT3-
377 like-3myc exhibits an electrophoretic mobility corresponding to a protein of 48.3 kDa,
378 which is expected considering the extra amino acids of the three copies of the c-Myc
379 epitope at the C-terminus. **c** and **d** H4 cells grown in glass coverslips were transfected to
380 express SIRT3-like-3myc (green channel) and incubated with MitoTracker Orange (red
381 channel in c) or mock incubated (d). Cells were fixed, permeabilized, and double- (c) or
382 triple-labeled (d) with mouse monoclonal antibody against the c-Myc epitope (c and d),
383 rabbit polyclonal antibody against the endoplasmic reticulum protein P63 (d) and sheep
384 polyclonal antibody against the Golgi apparatus protein TGN46 (c and d). Secondary
385 antibodies were Alexa-Fluor-488-conjugated donkey anti-mouse IgG (green channel),
386 Alexa-Fluor-594-conjugated donkey anti-rabbit IgG (red channel), and Alexa-Fluor-647-
387 conjugated donkey anti-sheep IgG (blue channel), and nuclei were stained with DAPI
388 (white channel). Stained cells were examined by fluorescence microscopy. Insets: X3
389 magnification with yellow arrows indicating colocalization (c) and green and red arrows
390 indicating lack of colocalization (d). Bar, 10 μm.
391

392 ## Elephant shark SIRT3-like protein has deacetylase activity

393 Reversible lysine acetylation is one of the most common post-translational modifications
394 on proteins that regulate a variety of physiological processes including gene expression,
395 enzymatic activity, protein-protein interactions, and subcellular localization (Glozak et al.
396 2005). Sirtuin proteins share a catalytic core domain (North and Verdin 2004) that have
397 NAD^+-dependent deacetylase activity (Shahgaldi and Kahmini 2021). After translocation
398 into the mitochondrial matrix, human SIRT3 is inactive, but after proteolytic processing of
399 its N-terminus signal peptide it becomes active as deacetylase (Onyango et al. 2002;
400 Schwer et al. 2002). Similar to human SIRT3, secondary structure prediction of
401 representative SIRT3-like proteins indicates that the first ~100 N-terminal amino acids are
402 in a disordered domain (data not shown). Therefore, to determine if SIRT3-like proteins
403 also exhibit deacetylase activity, we produced in bacteria N-terminal truncated elephant
404 shark SIRT3-like protein (amino acids 95-372; **Δ**NT-SIRT3-like). To analyze the
405 enzymatic activity of purified **Δ**NT-SIRT3-like, we used a commercial fluorometric

406 deacetylation activity assay that contains an acetylated substrate peptide for recombinant
407 human SIRT3 (Abcam). An initial analysis of activity at 37ºC showed that **Δ**NT-SIRT3-like
408 possesses a deacetylase activity that is similar to that of human SIRT3, being also NAD^+-
409 dependent (Fig. 9a, e, f). Because the enzymatic activity of elephant shark SIRT3-like
410 could be influenced by the environmental conditions, we next evaluated the optimal
411 temperature of **Δ**NT-SIRT3-like compared to that of human SIRT3. As expected, the
412 optimal temperature of the human SIRT3 was ~37ºC (Fig. 9b). In contrast, **Δ**NT-SIRT3-
413 like exhibited an optimal temperature at ~24ºC (Fig. 9b). The optimal temperature value
414 for the SIRT3-like deacetylase activity of the elephant shark could represent an
415 evolutionary adjustment to the temperature regime of the habitat in which this species
416 lives, as it has been demonstrated for other enzymes in other species (McCormick 1993;
417 Somero 2004; Bilyk et al. 2021; Saravia et al. 2021). Thus, all subsequent enzymatic
418 activity analyses for **Δ**NT-SIRT3-like were performed at 24ºC. The apparent specific
419 activity of **Δ**NT-SIRT3-like was 260.7 ± 9.9 fluorescence units (FU) min^{-1} mg^{-1}, which was
420 significantly lower than that of SIRT3 that was 1143.3 ± 46.3 FU min^{-1} mg^{-1}. Apparent K_m
421 of **Δ**NT-SIRT3-like and SIRT3 were 5.7 and 5.5, respectively, which resulted not
422 significantly different (Fig. 9c, d). In contrast, apparent V_{max} of **Δ**NT-SIRT3-like was 0.322
423 FU sec^{-1}, which was significantly different to that of SIRT3 that was 3.908 FU sec^{-1} (Fig.
424 9c, d). We next compared the effect of the sirtuin inhibitors nicotinamide (NAM) (Sauve
425 and Schramm 2003) and quercetin (QUE) (You et al. 2019) on the activities of SIRT3 and
426 **Δ**NT-SIRT3-like. As expected, SIRT3 activity was significantly inhibited by NAM and QUE
427 (Fig. 9e). We also found a significant inhibitory effect of both NAM and QUE on the activity
428 of **Δ**NT-SIRT3-like (Fig. 9f). We also compared the effect of the polyphenolic antioxidant
429 resveratrol (REV), which is an activator of sirtuins (Wood et al. 2004). As expected, we
430 found a significant concentration-dependent activation of SIRT3 deacetylase activity up
431 to a 1.6 ± 0.1-fold increase in the presence of 100 μM REV (Fig. 9e). Strikingly, we found
432 a much potent concentration dependent activation effect of REV on **Δ**NT-SIRT3-like,
433 showing up to a 11.1 ± 0.6 fold increase in the presence of 100 μM REV (Fig. 9f).
434 However, because the specific activity of **Δ**NT-SIRT3-like was ~23% that of SIRT3 in the
435 assay conditions, the activation of **Δ**NT-SIRT3-like by REV in fact represents a value only
436 ~1.6 fold higher compared to the activation of SIRT3 by REV. Because different sirtuins

437 have activity on different proteins, as well as remove with different specificity a variety of
438 acyl groups other than the acetyl (Fig. 1) (Anderson et al. 2014), the modulation of ΔNT-
439 SIRT3-like activity by REV suggests that it has distinct functional substrates. Together,
440 these results demonstrate that elephant shark ΔNT-SIRT3-like has deacetylase activity
441 and indicate that the activity of SIRT3-like proteins is modulated in a similar manner to
442 that of mammalian sirtuins.

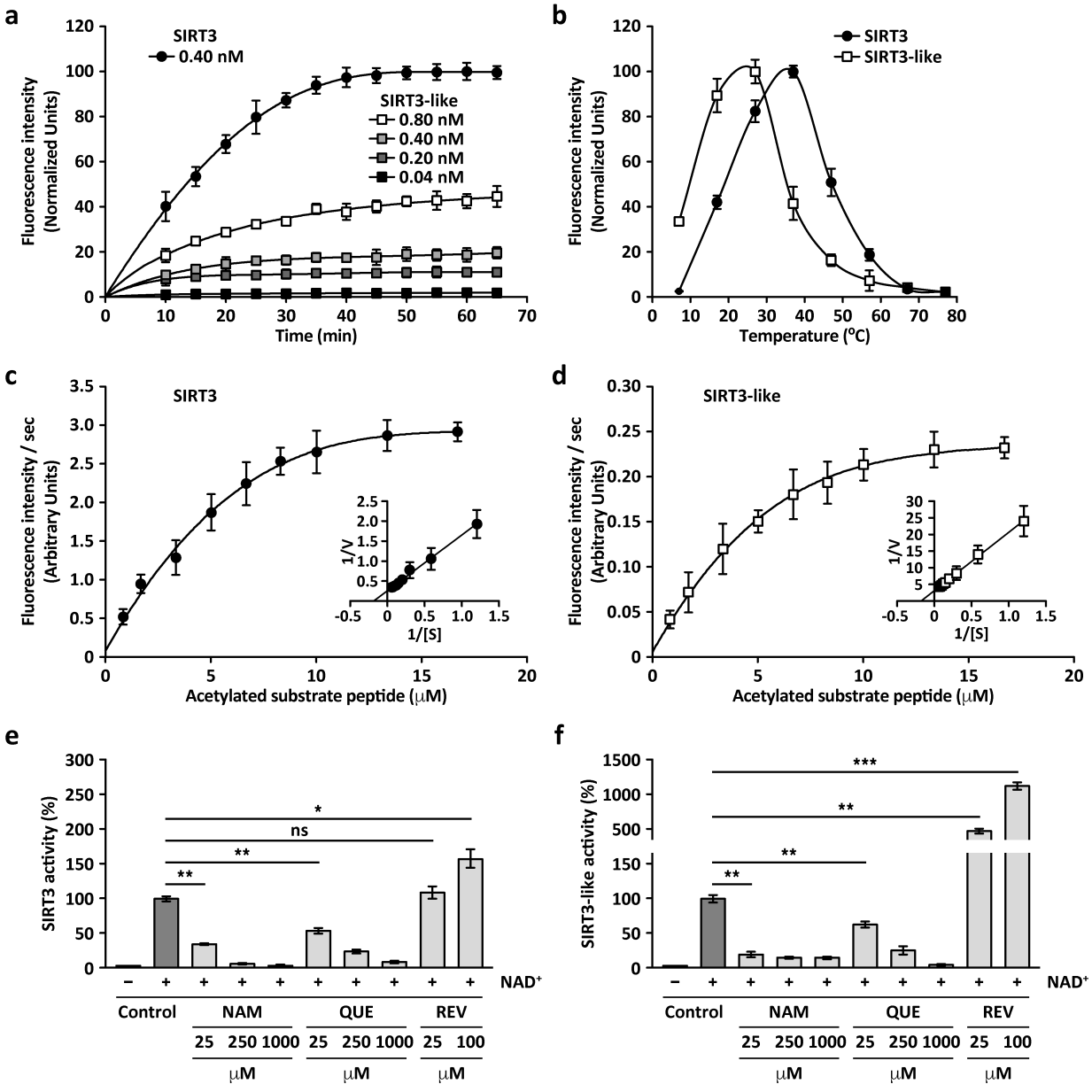

443
444
445

446 **Figure 9.** Comparison of deacetylase activity between human SIRT3 and elephant shark
447 **Δ**NT-SIRT3-like. a-f) Results obtained with a fluorometric deacetylation assay of an
448 acetylated substrate peptide. a) Time course of deacetylase activity at the indicated
449 concentration of SIRT3 and concentrations of **Δ**NT-SIRT3-like. b) Temperature
450 dependence of deacetylase activity. c-d) Michaelis-Menten plot and Lineweaver-Burk plot
451 of SIRT3 (c) and **Δ**NT-SIRT3-like (d) deacetylase activity. e-f) NAD^+ dependence and
452 concentration dependent effects of the SIRT3 inhibitors nicotinamide (NAM) and
453 quercetin (QUE) and of the SIRT3 activator resveratrol (REV) on the deacetylase activity
454 of SIRT3 (e) and **Δ**NT-SIRT3-like (f). In a-d, graphs depict the mean ± standard deviation
455 (n = 3). In e-f, bars represent the mean ± standard deviation. Statistical analysis was
456 performed using two-tailed unpaired Student's t-test (n = 3; * $p < 0.05$; ** $p < 0.01$; *** $p <$
457 0.001; ns, not statistically significant).
458

459 ## Elephant shark SIRT3-like protein increases ATP cellular content

460 Considering that SIRT3 plays an important role in maintaining basal ATP levels by
461 deacetylation of mitochondrial proteins involved in electron transport chain (ETC), the
462 tricarboxylic acid cycle, and fatty-acid oxidation (Hirschey et al. 2010), we investigated
463 the impact of transient SIRT3-like-3myc expression on ATP cellular content in H4 and
464 HeLa cells (Fig. 10a). Similar to the well-known effect of mammalian SIRT3, SIRT3-like-
465 3myc expression increased ATP cellular content, suggesting that it shares with SIRT3 the
466 ability to enhance the activity of the mitochondrial ETC. Because an enhancement in the
467 activity of ETC can cause an increase in reactive oxygen species (ROS), we also
468 evaluated the levels of ROS in cells expressing SIRT3-like-3myc (Fig. 10b). We found
469 similar ROS levels in cells expressing SIRT3-like-3myc and untransfected cells (Fig. 10b).
470 This finding suggests that SIRT3-like proteins share the mammalian SIRT3 characteristic
471 of protection against oxidative damage (Bause and Haigis 2013), likely by deacetylation
472 of enzymes involved in ROS clearance to protect mitochondrial membranes from
473 oxidative stress (Tseng et al. 2013). A candidate that could be activated by the
474 deacetylation activity of SIRT3-like proteins is SOD2 that in human cells reduces cellular
475 ROS content promoting oxidative stress resistance (Qiu et al. 2010; Tao et al. 2010).
476 Alternatively, SIRT3-like proteins could activate the last complex of the ETC by

477 deacetylation, enhancing ATP-synthase activity without affecting ROS production, similar
478 to the effect that SIRT3 has in response to exercise-induced stress (Vassilopoulos et al.
479 2014). Together, our results show that the SIRT3-like protein is a new sirtuin family
480 member with deacetylase activity that could have important roles in the homeostasis of
481 oxidative species and mitochondrial metabolism.

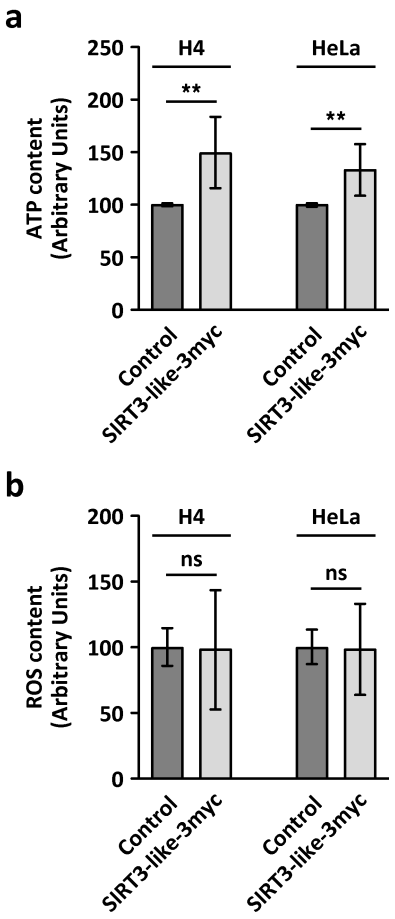

482

483

484 **Figure 10.** SIRT3-like-3myc expression causes an increment on ATP cellular
485 content with no difference in ROS levels. (a) ATP levels were measured by a
486 luciferin/luciferase bioluminescence assay in H4 and HeLa cells either left untreated
487 (Control) or transiently expressing SIRT3-like-3myc. (b) ROS content was measured by
488 the intensity fluorescence of the dye CM-H2DCFDA in H4 and HeLa cells either left
489 untreated (Control) or transiently expressing SIRT3-like-3myc. Bars represent the mean
490 ± standard deviation. Statistical analysis was performed using two-tailed unpaired
491 Student's t-test (n = 4; ** $p < 0.01$; ns, not statistically significant).

492

493 Conclusions

494 We performed an evolutionary analysis of the sirtuin gene family in vertebrates. In
495 addition to describing the duplicative history of sirtuins, our phylogenetic analyses
496 revealed the presence of a new gene family member, SIRT3-like. This new gene lineage
497 is present in all vertebrates other than mammals, birds, and reptiles. Furthermore, our
498 transcriptomic analyses show that SIRT3-like is transcribed in almost all examined
499 tissues, showing a tendency to be more expressed in the ovary, suggesting biological
500 functions related to reproduction. According to our analyses, SIRT3-like, localized in the
501 mitochondria, had deacetylase activity and increased the ATP cellular content. The
502 finding of a new sirtuin gene lineage highlights the need for more detailed assessments
503 of orthology with a more broad taxonomic sampling to better define the membership
504 composition of gene families (Glover et al. 2019). In the literature, there are examples in
505 which more comprehensive analyses provide a better description of gene families,
506 including previously unknown family members (Castro et al. 2012; Wichmann et al. 2016;
507 Céspedes et al. 2017; Ramos-Vicente et al. 2018; Opazo, Kuraku, et al. 2019; Opazo,
508 Hoffmann, et al. 2019). The availability of species with different gene repertoires could be
509 seen as a natural experiment (Albertson et al. 2009) that helps us understand the
510 evolutionary fate of duplicated genes, as they can fulfill the biological functions associated
511 with the gene family but with a different combination of paralogs.
512

513 **Methods**

514 Protein sequences and phylogenetic analyses

515 We retrieved sirtuin amino acid sequences in representative species of all main groups
516 of vertebrates. Our sampling included mammals, birds, reptiles, amphibians, coelacanth,
517 bony fish, cartilaginous fish, and cyclostomes (Supplementary Table S1). Sequences
518 were obtained from the Orthologous MAtrix project (OMA), December 2021 release
519 (Altenhoff et al. 2021)(last accessed on April 8th, 2022). In addition, we complemented
520 our sampling by retrieving sequences from vertebrate groups that were not present or
521 poorly represented in the Orthologous MAtrix project (e.g., crocodiles) from the National
522 Center for Biotechnology Information (NCBI) (Sharma et al. 2019) using the program blast
523 (tblastn) with default parameters (Altschul et al. 1990)(Supplementary Table S1). Protein
524 sequences were aligned using the software MAFFT v.7 (Katoh and Standley 2013),

525 allowing the program to choose the alignment strategy (FFT-NS-i). To select the best-
526 fitting model of molecular evolution we used the proposed model tool in the program IQ-
527 Tree v1.6.12 (Kalyaanamoorthy et al. 2017), which selected JTT+F+I+G4. We used a
528 maximum-likelihood approach to obtain the best tree using the program IQ-Tree v1.6.12
529 (Trifinopoulos et al. 2016). We carried out 20 independent runs to explore the tree space
530 changing the value of the strength of the perturbation (-pers) parameter. We conducted
531 the following analyses:

532 1. Five runs modifying the strength of the perturbation parameter from 0.5 (default
533 value) to 0.3.
534 2. Five runs using the default value (0.5) for the strength of the perturbation
535 parameter.
536 3. Five runs modifying the strength of the perturbation parameter from 0.5 (default
537 value) to 0.7.
538 4. Five runs modifying the strength of the perturbation parameter from 0.5 (default
539 value) to 0.9.

540 In all cases, the number of unsuccessful iterations to stop parameter (-nstop) value was
541 changed from 100 (default value) to 500. The tree with the highest likelihood score was
542 chosen (log-likelihood: -127052.963, -pers 0.5 and -nstop 500). Support for the nodes
543 was evaluated using two approaches: the aBayes test (Anisimova et al. 2011) and the
544 ultrafast bootstrap procedure (Hoang et al. 2018). Nicotinamide Nucleotide
545 Transhydrogenase (NNT) protein sequences from the human (*Homo sapiens*), mouse
546 (*Mus musculus*), zebrafish (*Danio rerio*) and spotted gar (*Lepisosteus oculatus*) were
547 used as outgroups.
548

549 ## Assessment of conserved synteny

550 We examined genes found upstream and downstream of the sirtuin genes. For
551 comparative purposes, we used the estimates of orthology and paralogy derived from the
552 Ensembl Compara database (Herrero et al. 2016); these estimates are obtained from a
553 pipeline that considers both synteny and phylogeny to generate orthology mappings.
554 These predictions were visualized using the program Genomicus v100.01 (Nguyen et al.
555 2018). Our assessments were performed in humans (*Homo sapiens*), chicken (*Gallus*

556 *gallus*), gharial (*Gavialis gangeticus*), red-eared slider (*Trachemys scripta*), green anole
557 (*Anolis carolinensis*), tropical clawed frog (*Xenopus tropicalis*), coelacanth (*Latimeria*
558 *chalumnae*), spotted gar (*Lepisosteus oculatus*), and elephant shark (*Callorhinchus milii*).
559

560 ## Dot-plots

561 We retrieved the chromosomal region containing the SIRT3-like gene of the tropical
562 clawed frog (*Xenopus tropicalis*, Ch3) including 6.7 kb up- and downstream, and the
563 corresponding syntenic region in the human (*Homo sapiens*, Chr12), opossum
564 (*Monodelphis domestica*, Chr8), chicken (*Gallus gallus*, Chr1), gharial (*Gavialis*
565 *gangeticus*, NW_017729022.1), red-eared slider (*Trachemys scripta*, Chr1), and green
566 anole (*Anolis carolinensis*, Chr5) based on the location of the flanking genes (RIC8B and
567 TMEM263). We aligned SIRT3-like syntenic regions using Advanced PipMaker (Schwartz
568 et al. 2000).
569

570 ## Transcript abundance analyses

571 Sirtuin transcript abundance was measured from a representative sample of vertebrates
572 including the elephant shark (*Callorhinchus milii*), zebrafish (*Danio rerio*), tropical clawed
573 frog (*Xenopus tropicalis*), anole lizard (*Anolis carolinensis*), and human (*Homo sapiens*).
574 RNASeq libraries from brain, heart, kidney, liver, muscle, ovary, and testis from each
575 species were gathered from the NCBI Short Read Archive (SRA)(Leinonen et al. 2011).
576 Accession numbers for species and tissue specific libraries can be found in Supplemental
577 Table S2. Reference transcript sequences were collected from Ensembl v.100 (Yates et
578 al. 2020) and we removed sequences that were shorter than 100 bp. For each library
579 adapters were removed using Trimmomatic 0.38 (Bolger et al. 2014) and reads were
580 filtered for quality using the parameters HEADCROP:5, SLIDINGWINDOW:5:30, and
581 MINLEN:50. We mapped quality filtered paired-end RNAseq reads back to reference
582 sequences using Bowtie 1.2.2 (Langmead et al. 2009) and default parameters of RSEM
583 (Li and Dewey 2011). Transcripts with < 10 mapped reads across all seven tissues per
584 species were removed prior to normalization. Normalization of raw read counts for each
585 species was performed using the estimateSizeFactors and estimateDispersions functions

586 in DESeq2 v1.26 (Love et al. 2014). If multiple SIRT transcripts were present, we
587 presented the expression data from the transcript with the most mapped reads.
588

589 Protein structure homology modeling

590 Protein structure homology modeling was performed using the SWISS-MODEL server
591 (https://swissmodel.expasy.org/) (Waterhouse et al. 2018). Structural figures were
592 prepared with PyMOL Molecular Graphics System, Version 2.0.6 Schrödinger, LLC.
593

594 Recombinant cDNA Constructs

595 For expression in mammalian cells, a codon-optimized mammalian expression construct
596 encoding full-length (amino acids 1-372) elephant shark (*Callorhinchus milii*) SIRT3-like
597 (Supplementary table S1), cloned in-frame into the *Eco*RI and *Sal*I sites of the pCMV-
598 3Tag-4a vector followed by vector encoding sequence of three successive Myc epitope
599 tags before a stop codon, was acquired from GenScript (Piscataway, NJ). For the
600 generation of a codon-optimized bacterial expression construct, a cDNA encoding N-
601 terminal truncated (amino acids 95-372) elephant shark SIRT3-like, cloned in-frame into
602 the *Eco*RI and *Sal*I sites of the pGEX-4T-1 vector, was also acquired from GenScript.
603 This cDNA was subsequently cloned in-frame into the *Eco*RI and *Sal*I sites of the pGST-
604 Parallel-1 vector (Sheffield et al. 1999). The nucleotide sequence of all recombinant
605 constructs was confirmed by dideoxy sequencing using the AUSTRAL-omics core facility
606 at Universidad Austral de Chile (https://australomics.cl/).
607

608 Cell culture, cell transfection and preparation of protein extracts

609 H4 human neuroglioma cells, HeLa human cervix adenocarcinoma cells and MDA-MB-
610 231 human mammary gland adenocarcinoma cells were obtained from the American
611 Type Culture Collection (Manassas, VA). H4 and HeLa cells were maintained in
612 Dulbecco's modified Eagle's medium (DMEM), and MDA-MB-231 in DMEM-F12
613 (ThermoFisher, Waltham, MA). For all cell lines, media were supplemented with 10%
614 heat-inactivated fetal bovine serum, 100 U/ml penicillin, 100 µg/ml streptomycin
615 (ThermoFisher), and 5 µg/ml plasmocin (InvivoGen, San Diego, CA), and cells were
616 cultured in a humidified incubator with 5% CO_2 at 37 °C. For transient transfections, cells

617 were either seeded on top of glass coverslips on 24-well plates or on 6-well plates. When
618 cells were ~60% confluent, transfections were performed with Lipofectamine 2000
619 (ThermoFisher), according to the manufacturer's instructions. Preparation of protein
620 extracts from cultured, transfected or non-transfected cells was performed using methods
621 described elsewhere (Tenorio et al. 2016).
622

623 Antibodies and cell reagents

624 We used the following antibodies: mouse clone 9E10 to the c-Myc epitope (Covance,
625 Princeton, NJ), mouse clone BA3R to β-actin (ThermoFisher), rabbit polyclonal to p63
626 (Merck, Germany; cat # HPA001225), and sheep polyclonal to TGN46 (Bio-Rad
627 Laboratories, Hercules, CA; cat # AHP500G). The following fluorochrome-conjugated
628 antibodies were from ThermoFisher: Alexa Fluor-488–conjugated donkey anti mouse
629 IgG, Alexa Fluor-594–conjugated donkey anti rabbit IgG and Alexa Fluor-647-conjugated
630 donkey anti sheep IgG. HRP-conjugated secondary antibodies were from Jackson
631 ImmunoResearch (West Grove, PA). Depending on their reactivity, primary antibodies
632 were used at a dilution 1/200 to 1/2000. HRP-conjugated secondary antibodies were used
633 at dilutions 1/5000 to 1/20000 also depending on their reactivity. All Alexa Fluor-
634 conjugated secondary antibodies were used at a dilution 1/1000. The fluorescent nuclear
635 stain 4',6-diamidino-2-phenylindole (DAPI) was also from ThermoFisher.
636

637 Protein Electrophoresis, Immunoblotting and Immunofluorescence
638 Microscopy

639 SDS-PAGE and immunoblotting were performed as described (Bustamante et al. 2020).
640 For fluorescence microscopy, cells grown on glass coverslips were transfected, and after
641 16-h cells were left untreated or treated for 30 min with MitoTracker™ Orange CMTMRos
642 (ThermoFisher) according to the manufacturer's instructions. After washing with
643 phosphate buffered saline (PBS) supplemented with 0.1 mM $CaCl_2$ and 1 mM $MgCl_2$
644 (PBS-CM), cells were fixed in 4% paraformaldehyde for 30 min at room temperature,
645 permeabilized with 0.2% Triton X-100 in PBS-CM for 15 min at room temperature, and
646 incubated with blocking solution (0.2% gelatin in PBS-CM) for 10 min at room
647 temperature. Cells were incubated simultaneously either with antibodies to the c-Myc

648 epitope (1/200) and to TGN46 (1/1000) or to the c-Myc epitope, to TGN46 and to p63
649 (1/600) for 30 min at 37 ºC in a humidified chamber. After washing coverslips with PBS,
650 cells were incubated as before, but with fluorochrome-conjugated antibodies, followed by
651 PBS-washing, and coverslips were mounted onto glass slides with Fluoromount-G
652 mounting medium (ThermoFisher). Fluorescence microscopy images were acquired with
653 an AxioObserver.D1 microscope equipped with a PlanApo 63x oil immersion objective
654 (NA 1.4), and an AxioCam MRm digital camera (Carl Zeiss). To prepare figures, 12-bit
655 images were processed with ImageJ software (version 1.44o; Wayne Rasband, NIH,
656 http://imagej.nih.gov) and Adobe Photoshop CS3 software (Adobe Systems, Mountain
657 View, CA).
658

659 ## Expression and Purification of Recombinant N-terminal truncated elephant
660 shark SIRT3-like protein

661 Recombinant, N-terminal truncated elephant shark SIRT3-like (**Δ**NT-SIRT3-like; amino
662 acids 95-372) tagged with an N-terminal glutathione S-transferase (GST) followed by a
663 tobacco etch virus (TEV) protease cleavage site was expressed and purified using a
664 method described previously (Ross et al. 2014), with some modifications. Briefly,
665 expression in *E. coli* B834(DE3) (Novagen, Madison, WI) was induced with 0.25 mM IPTG
666 at 25 °C for 16 h. Pellets of bacteria were resuspended in homogenization buffer (50 mM
667 Tris HCl, 0.5 M NaCl, 5 mM EDTA, 5 mM β-mercaptoethanol, and 2 mM
668 phenylmethylsulfonyl fluoride, pH 8.0) and lysed by sonication. The clarified supernatant
669 was purified on glutathione-Sepharose 4B (GE Healthcare). After removal of the GST
670 moiety by TEV cleavage, and sequential further passage through glutathione-Sepharose
671 4B and Ni-NTA (QIAGEN) resins, **Δ**NT-SIRT3-like was further purified on a Superdex 200
672 column (GE Healthcare) equilibrated in storage buffer (50 mM Tris HCl, 150 mM NaCl, 1
673 mM DTT). Aliquots of purified protein were kept at -80 ºC until use.
674

675 ## Deacetylation activity

676 To characterize deacetylation activity of recombinant, N-terminal truncated elephant
677 shark SIRT3-like protein (**Δ**NT-SIRT3-like), we used a fluorometric SIRT3 activity assay
678 kit (Abcam, cat # ab156067; Cambridge, UK), according to the manufacturer's

679 instructions. This assay allows detection of a fluorescent signal upon deacetylation of an
680 acetylated substrate peptide for recombinant human SIRT3. The intensity of fluorescence
681 was measured on a fluorometric microplate reader (Varioskan Flash, ThermoFisher) with
682 excitation set at 350 nm and emission detection set at 450 nm. To analyze the
683 deacetylation activity of N-terminal truncated elephant shark SIRT3-like protein, first we
684 determined its optimum temperature that resulted to be ~24 ºC. Subsequent analyses
685 were performed by comparing the activity of N-terminal truncated elephant shark SIRT3-
686 like protein at 24 ºC to that of human SIRT3, which is provided by the assay kit, at 37 ºC.
687 K_m and V_{max} were obtained by varying the concentration of the fluorogenic acetylated
688 substrate peptide provided by the assay kit. This assay was also used to determine the
689 effect of nicotinamide (NAM), quercetin (QUE) and resveratrol (REV; Sigma-Aldrich) on
690 the deacetylation activity of ΔNT-SIRT3-like.
691

692 ## ATP and ROS content

693 ATP levels were quantified in cell lysates using a luciferin/luciferase bioluminescence
694 assay (ATP determination kit, Molecular Probes cat # A22066, Thermo Fisher Scientific)
695 as previously described (Jara et al. 2018). Briefly, cells were lysed in HEPES buffer (125
696 mM NaCl, 25 mM NaF, 1 mM EDTA, 1 mM EGTA, 1% NP-40, 25 mM HEPES, pH 7.4)
697 supplemented with a protease inhibitor mixture (cat # 78429, Thermo Fisher Scientific)
698 and centrifuged at 12000 rpm using a refrigerated centrifuge (Eppendorf model 5424R)
699 for 15 min at 4 ºC. Proteins in the supernatant were quantified, and 10 µl of lysate were
700 used to determine ATP levels according to the kit manufacturer's instructions. The ATP
701 level in each sample was calculated using standard curves and normalized to the protein
702 concentration in each sample. ROS content was determined in cell lysates using 25 µM
703 CM-H2DCFDA (DCF; a fluorogenic indicator of ROS), as previously described (Jara et
704 al. 2018; Olesen et al. 2020). The intensity of fluorescence was measured on a
705 fluorescence plate reader (Biotek Synergy HT, Agilent, Santa Clara, CA) with excitation
706 set at 485 nm and emission detection set at 530 nm. Briefly, in a dark 96-well plate, 25
707 µg of cell lysate proteins were incubated with CM-H2DCFDA (DCF) dye with shaking for
708 5 min at room temperature, followed by determination of the fluorescence of each sample
709 that was subtracted by the fluorescence of the respective blank.

Statistical Analysis

In the case of the deacetylation, ATP content and ROS content assays, quantification was performed from at least three independent experiments/measurements. Statistical analysis was performed using Microsoft Excel for Mac 2011 (Microsoft Corporation). When appropriate, results are represented in graphs depicting the mean ± standard deviation. Statistical significance was determined by two-tailed, paired t-test. P-values > 0.05 or ≤ 0.05 were regarded as not statistically significant or statistically significant, respectively. In the figures, P-values between 0.01 and 0.05 are indicated with one asterisk, P-values between 0.001 and 0.01 are indicated with two asterisks, and P-values less than 0.001 are indicated with three asterisks.

Data accessibility

Data and supplementary material are available online:

Acknowledgements

This work was supported by the Fondo Nacional de Desarrollo Científico y Tecnológico from Chile (FONDECYT 1210471) and Millennium Nucleus of Ion Channels Associated Diseases (MiNICAD), Iniciativa Científica Milenio, Ministry of Economy, Development and Tourism from Chile to JCO, Fondo Nacional de Desarrollo Científico y Tecnológico from Chile (FONDECYT 1211481) to GAM, National Science Foundation (EPS-0903787, DBI-1262901 and DEB-1354147) to F.G.H., Financiamiento Basal No. ANID/BASAL/ACE210009 to PVB and No. ANID/BASAL/FB210008 to PVB and CTR, Fondap-Ideal Grant N° 15150003 to LV-C, ANID-Millennium Science Initiative Program-Center ICM-ANID ICN2021_002 to LV-C, Fondo Nacional de Desarrollo Científico y Tecnológico from Chile (FONDECYT 1180957) to FJM, Vicerrectoría de Investigación, Desarrollo y Creación Artística, Universidad Austral de Chile to JCO, FJM, LVC, GAM. We thank Stefanie Teuber, John Quiroga and Rafael Burgos, Instituto de Farmacología y Morfofisiología, Facultad de Ciencias Veterinarias, Universidad Austral de Chile, for

739 providing assistance in the use of the Varioskan Flash microplate reader; Hianara
740 Bustamante, Instituto de Microbiología Clínica, Facultad de Medicina, Universidad
741 Austral de Chile, for providing quercetin and resveratrol; Víctor Castro, Departamento de
742 Biología, Facultad de Ciencias, Universidad de Chile, for providing NAD^+ and
743 nicotinamide; and Gonzalo Astroza, and Andrés Rivera-Dictter for technical assistance.
744

745 ## Contributions

746 JCO and GAM designed the study. JCO, MWV, FGH, KZ, CM, CL, VC, FJM, PVB, CTR,
747 GAM, collected and/or analyzed data. JCO, PVB and GAM wrote the manuscript. JCO,
748 MWV, FGH, KZ, CM, CL, VC, LV-C, FJM, PVB, CTR and GAM, reviewed and edited the
749 manuscript. All authors contributed to the article and approved the submitted version.
750

751 # Ethics declarations

752 ## Conflict of interest disclosure

753 The authors declare they have no conflict of interest relating to the content of this
754 article. Juan C. Opazo is a recommender for PCI Evol Biol and PCI Genomics.
755

756 ## Data availability

757 Data and supplementary material are available online at zenodo.org
758
759
760
761
762
763
764
765
766
767
768
769

References

Albalat R, Cañestro C. 2016. Evolution by gene loss. *Nat. Rev. Genet.* 17:379–391.

Albertson RC, Craig Albertson R, Cresko W, William Detrich H, Postlethwait JH. 2009. Evolutionary mutant models for human disease. *Trends in Genetics* [Internet] 25:74–81. Available from: http://dx.doi.org/10.1016/j.tig.2008.11.006

Altenhoff AM, Train C-M, Gilbert KJ, Mediratta I, Mendes de Farias T, Moi D, Nevers Y, Radoykova H-S, Rossier V, Warwick Vesztrocy A, et al. 2021. OMA orthology in 2021: website overhaul, conserved isoforms, ancestral gene order and more. *Nucleic Acids Res.* 49:D373–D379.

Altschul SF, Gish W, Miller W, Myers EW, Lipman DJ. 1990. Basic local alignment search tool. *J. Mol. Biol.* 215:403–410.

Anderson KA, Green MF, Huynh FK, Wagner GR, Hirschey MD. 2014. SnapShot: Mammalian Sirtuins. *Cell* 159:956–956.e1.

Anisimova M, Gil M, Dufayard J-F, Dessimoz C, Gascuel O. 2011. Survey of branch support methods demonstrates accuracy, power, and robustness of fast likelihood-based approximation schemes. *Syst. Biol.* 60:685–699.

Bause AS, Haigis MC. 2013. SIRT3 regulation of mitochondrial oxidative stress. *Exp. Gerontol.* 48:634–639.

Bilyk KT, Zhuang X, Vargas-Chacoff L, Cheng C-HC. 2021. Evolution of chaperome gene expression and regulatory elements in the antarctic notothenioid fishes. *Heredity* 126:424–441.

Bolger AM, Lohse M, Usadel B. 2014. Trimmomatic: a flexible trimmer for Illumina sequence data. *Bioinformatics* 30:2114–2120.

Brown K, Xie S, Qiu X, Mohrin M, Shin J, Liu Y, Zhang D, Scadden DT, Chen D. 2013. SIRT3 reverses aging-associated degeneration. *Cell Rep.* 3:319–327.

Bustamante HA, Cereceda K, González AE, Valenzuela GE, Cheuquemilla Y, Hernández S, Arias-Muñoz E, Cerda-Troncoso C, Bandau S, Soza A, et al. 2020. The Proteasomal Deubiquitinating Enzyme PSMD14 Regulates Macroautophagy by Controlling Golgi-to-ER Retrograde Transport. *Cells* [Internet] 9. Available from: http://dx.doi.org/10.3390/cells9030777

Castro LFC, Lopes-Marques M, Gonçalves O, Wilson JM. 2012. The evolution of pepsinogen C genes in vertebrates: duplication, loss and functional diversification. *PLoS One* 7:e32852.

Céspedes HA, Zavala K, Vandewege MW, Opazo JC. 2017. Evolution of the α-adrenoreceptors in vertebrates: ADRA2D is absent in mammals and crocodiles.

805 *Gen. Comp. Endocrinol.* 250:85–94.

806 Costantini S, Sharma A, Raucci R, Costantini M, Autiero I, Colonna G. 2013. Genealogy
807 of an ancient protein family: the Sirtuins, a family of disordered members. *BMC*
808 *Evol. Biol.* 13:60.

809 Delsuc F, Brinkmann H, Chourrout D, Philippe H. 2006. Tunicates and not
810 cephalochordates are the closest living relatives of vertebrates. *Nature* 439:965–
811 968.

812 Delsuc F, Tsagkogeorga G, Lartillot N, Philippe H. 2008. Additional molecular support
813 for the new chordate phylogeny. *Genesis* 46:592–604.

814 Di Emidio G, Falone S, Artini PG, Amicarelli F, D'Alessandro AM, Tatone C. 2021.
815 Mitochondrial Sirtuins in Reproduction. *Antioxidants (Basel)* [Internet] 10. Available
816 from: http://dx.doi.org/10.3390/antiox10071047

817 Félix M-A, Barkoulas M. 2015. Pervasive robustness in biological systems. *Nat. Rev.*
818 *Genet.* 16:483–496.

819 Frye RA. 2000. Phylogenetic classification of prokaryotic and eukaryotic Sir2-like
820 proteins. *Biochem. Biophys. Res. Commun.* 273:793–798.

821 Frye RA. 2006. Evolution of Sirtuins From Archaea to Vertebrates. *Histone*
822 *Deacetylases* [Internet]:183–202. Available from: http://dx.doi.org/10.1385/1-59745-
823 024-3:183

824 Fujita Y, Yamashita T. 2018. Sirtuins in Neuroendocrine Regulation and Neurological
825 Diseases. *Front. Neurosci.* 12:778.

826 Glover N, Dessimoz C, Ebersberger I, Forslund SK, Gabaldón T, Huerta-Cepas J,
827 Martin M-J, Muffato M, Patricio M, Pereira C, et al. 2019. Advances and
828 Applications in the Quest for Orthologs. *Mol. Biol. Evol.* 36:2157–2164.

829 Glozak MA, Sengupta N, Zhang X, Seto E. 2005. Acetylation and deacetylation of non-
830 histone proteins. *Gene* 363:15–23.

831 Goldberg T, Hecht M, Hamp T, Karl T, Yachdav G, Ahmed N, Altermann U, Angerer P,
832 Ansorge S, Balasz K, et al. 2014. LocTree3 prediction of localization. *Nucleic Acids*
833 *Res.* 42:W350–W355.

834 Greiss S, Gartner A. 2009. Sirtuin/Sir2 phylogeny, evolutionary considerations and
835 structural conservation. *Mol. Cells* 28:407–415.

836 Haigis MC, Sinclair DA. 2010. Mammalian sirtuins: biological insights and disease
837 relevance. *Annu. Rev. Pathol.* 5:253–295.

838 Hara Y, Yamaguchi K, Onimaru K, Kadota M, Koyanagi M, Keeley SD, Tatsumi K,

Tanaka K, Motone F, Kageyama Y, et al. 2018. Shark genomes provide insights into elasmobranch evolution and the origin of vertebrates. *Nat Ecol Evol* 2:1761–1771.

Helsen J, Voordeckers K, Vanderwaeren L, Santermans T, Tsontaki M, Verstrepen KJ, Jelier R. 2020. Gene Loss Predictably Drives Evolutionary Adaptation. *Mol. Biol. Evol.* 37:2989–3002.

Herrero J, Muffato M, Beal K, Fitzgerald S, Gordon L, Pignatelli M, Vilella AJ, Searle SMJ, Amode R, Brent S, et al. 2016. Ensembl comparative genomics resources. *Database* [Internet] 2016. Available from: http://dx.doi.org/10.1093/database/bav096

Himmel NJ, Gray TR, Cox DN. 2020. Phylogenetics Identifies Two Eumetazoan TRPM Clades and an Eighth TRP Family, TRP Soromelastatin (TRPS). *Mol. Biol. Evol.* 37:2034–2044.

Hirschey MD. 2011. Old enzymes, new tricks: sirtuins are NAD(+)-dependent de-acylases. *Cell Metab.* 14:718–719.

Hirschey MD, Shimazu T, Goetzman E, Jing E, Schwer B, Lombard DB, Grueter CA, Harris C, Biddinger S, Ilkayeva OR, et al. 2010. SIRT3 regulates mitochondrial fatty-acid oxidation by reversible enzyme deacetylation. *Nature* 464:121–125.

Hoang DT, Chernomor O, von Haeseler A, Minh BQ, Vinh LS. 2018. UFBoot2: Improving the Ultrafast Bootstrap Approximation. *Mol. Biol. Evol.* 35:518–522.

Howe KL, Achuthan P, Allen J, Allen J, Alvarez-Jarreta J, Amode MR, Armean IM, Azov AG, Bennett R, Bhai J, et al. 2021. Ensembl 2021. *Nucleic Acids Res.* 49:D884–D891.

Iwabe N, Hara Y, Kumazawa Y, Shibamoto K, Saito Y, Miyata T, Katoh K. 2005. Sister group relationship of turtles to the bird-crocodilian clade revealed by nuclear DNA-coded proteins. *Mol. Biol. Evol.* 22:810–813.

Jara C, Aránguiz A, Cerpa W, Tapia-Rojas C, Quintanilla RA. 2018. Genetic ablation of tau improves mitochondrial function and cognitive abilities in the hippocampus. *Redox Biol* 18:279–294.

Kabiljo J, Murko C, Pusch O, Zupkovitz G. 2019. Spatio-temporal expression profile of sirtuins during aging of the annual fish Nothobranchius furzeri. *Gene Expression Patterns* [Internet] 33:11–19. Available from: http://dx.doi.org/10.1016/j.gep.2019.05.001

Kalyaanamoorthy S, Minh BQ, Wong TKF, von Haeseler A, Jermiin LS. 2017. ModelFinder: fast model selection for accurate phylogenetic estimates. *Nat. Methods* 14:587–589.

875 Katoh K, Standley DM. 2013. MAFFT multiple sequence alignment software version 7:
876 improvements in performance and usability. *Mol. Biol. Evol.* 30:772–780.

877 Kumar S, Stecher G, Suleski M, Hedges SB. 2017. TimeTree: A Resource for
878 Timelines, Timetrees, and Divergence Times. *Mol. Biol. Evol.* 34:1812–1819.

879 Kuraku S. 2013. Impact of asymmetric gene repertoire between cyclostomes and
880 gnathostomes. *Semin. Cell Dev. Biol.* 24:119–127.

881 Langmead B, Trapnell C, Pop M, Salzberg SL. 2009. Ultrafast and memory-efficient
882 alignment of short DNA sequences to the human genome. *Genome Biol.* 10:R25.

883 Leinonen R, Sugawara H, Shumway M, International Nucleotide Sequence Database
884 Collaboration. 2011. The sequence read archive. *Nucleic Acids Res.* 39:D19–D21.

885 Li B, Dewey CN. 2011. RSEM: accurate transcript quantification from RNA-Seq data
886 with or without a reference genome. *BMC Bioinformatics* [Internet] 12. Available
887 from: http://dx.doi.org/10.1186/1471-2105-12-323

888 Love MI, Huber W, Anders S. 2014. Moderated estimation of fold change and
889 dispersion for RNA-seq data with DESeq2. *Genome Biol.* 15:550.

890 Lynch M, Conery JS. 2000. The Evolutionary Fate and Consequences of Duplicate
891 Genes. *Science* [Internet] 290:1151–1155. Available from:
892 http://dx.doi.org/10.1126/science.290.5494.1151

893 McCormick SD. 1993. Methods for nonlethal gill biopsy and measurement of Na+, K+-
894 ATPase activity. *Can. J. Fish. Aquat. Sci.* 50:656–658.

895 McDonnell E, Peterson BS, Bomze HM, Hirschey MD. 2015. SIRT3 regulates
896 progression and development of diseases of aging. *Trends Endocrinol. Metab.*
897 26:486–492.

898 Michan S, Sinclair D. 2007. Sirtuins in mammals: insights into their biological function.
899 *Biochem. J* 404:1–13.

900 Nei M, Rooney AP. 2005. Concerted and birth-and-death evolution of multigene
901 families. *Annu. Rev. Genet.* 39:121–152.

902 Nguyen NTT, Vincens P, Roest Crollius H, Louis A. 2018. Genomicus 2018: karyotype
903 evolutionary trees and on-the-fly synteny computing. *Nucleic Acids Res.* 46:D816–
904 D822.

905 North BJ, Verdin E. 2004. Sirtuins: Sir2-related NAD-dependent protein deacetylases.
906 *Genome Biol.* 5:224.

907 Ohno S. 1985. Dispensable genes. *Trends Genet.* 1:160–164.

908 Olesen MA, Torres AK, Jara C, Murphy MP, Tapia-Rojas C. 2020. Premature synaptic
909 mitochondrial dysfunction in the hippocampus during aging contributes to memory
910 loss. *Redox Biol* 34:101558.

911 Olson MV. 1999. When less is more: gene loss as an engine of evolutionary change.
912 *Am. J. Hum. Genet.* 64:18–23.

913 Onyango P, Celic I, McCaffery JM, Boeke JD, Feinberg AP. 2002. SIRT3, a human
914 SIR2 homologue, is an NAD-dependent deacetylase localized to mitochondria.
915 *Proc. Natl. Acad. Sci. U. S. A.* 99:13653–13658.

916 Opazo JC, Hoffmann FG, Zavala K, Edwards SV. 2019. Evolution of the DAN gene
917 family in vertebrates. *Evolutionary Biology*:185.

918 Opazo JC, Kuraku S, Zavala K, Toloza-Villalobos J, Hoffmann FG. 2019. Evolution of
919 nodal and nodal-related genes and the putative composition of the heterodimers
920 that trigger the nodal pathway in vertebrates. *Evolution & Development* [Internet]
921 21:205–217. Available from: http://dx.doi.org/10.1111/ede.12292

922 Opazo JC, Vandewege MW, Gutierrez J, Zavala K, Vargas-Chacoff L, Morera FJ,
923 Mardones GA. 2021. Independent duplications of the Golgi phosphoprotein 3
924 oncogene in birds. *Sci. Rep.* 11:12483.

925 Pereira TCB, Rico EP, Rosemberg DB, Schirmer H, Dias RD, Souto AA, Bonan CD,
926 Bogo MR. 2011. Zebrafish as a model organism to evaluate drugs potentially able
927 to modulate sirtuin expression. *Zebrafish* 8:9–16.

928 Qiu H, Hildebrand F, Kuraku S, Meyer A. 2011. Unresolved orthology and peculiar
929 coding sequence properties of lamprey genes: the KCNA gene family as test case.
930 *BMC Genomics* 12:325.

931 Qiu X, Brown K, Hirschey MD, Verdin E, Chen D. 2010. Calorie restriction reduces
932 oxidative stress by SIRT3-mediated SOD2 activation. *Cell Metab.* 12:662–667.

933 Rajabi N, Galleano I, Madsen AS, Olsen CA. 2018. Targeting Sirtuins: Substrate
934 Specificity and Inhibitor Design. *Prog. Mol. Biol. Transl. Sci.* 154:25–69.

935 Ramos-Vicente D, Ji J, Gratacòs-Batlle E, Gou G, Reig-Viader R, Luís J, Burguera D,
936 Navas-Perez E, García-Fernández J, Fuentes-Prior P, et al. 2018. Metazoan
937 evolution of glutamate receptors reveals unreported phylogenetic groups and
938 divergent lineage-specific events. *Elife* [Internet] 7. Available from:
939 http://dx.doi.org/10.7554/eLife.35774

940 Ross BH, Lin Y, Corales EA, Burgos PV, Mardones GA. 2014. Structural and functional
941 characterization of cargo-binding sites on the μ4-subunit of adaptor protein complex
942 4. *PLoS One* 9:e88147.

943 Saravia J, Paschke K, Oyarzún-Salazar R, Cheng C-HC, Navarro JM, Vargas-Chacoff

944 L. 2021. Effects of warming rates on physiological and molecular components of
945 response to CTMax heat stress in the Antarctic fish Harpagifer antarcticus. *J.*
946 *Therm. Biol.* 99:103021.

947 Sauve AA, Schramm VL. 2003. Sir2 regulation by nicotinamide results from switching
948 between base exchange and deacetylation chemistry. *Biochemistry* 42:9249–9256.

949 Scher MB, Vaquero A, Reinberg D. 2007. SirT3 is a nuclear NAD+-dependent histone
950 deacetylase that translocates to the mitochondria upon cellular stress. *Genes Dev.*
951 21:920–928.

952 Scholte LLS, Mourão MM, Pais FS-M, Melesina J, Robaa D, Volpini AC, Sippl W, Pierce
953 RJ, Oliveira G, Nahum LA. 2017. Evolutionary relationships among protein lysine
954 deacetylases of parasites causing neglected diseases. *Infect. Genet. Evol.* 53:175–
955 188.

956 Schwartz S, Zhang Z, Frazer KA, Smit A, Riemer C, Bouck J, Gibbs R, Hardison R,
957 Miller W. 2000. PipMaker--a web server for aligning two genomic DNA sequences.
958 *Genome Res.* 10:577–586.

959 Schwer B, North BJ, Frye RA, Ott M, Verdin E. 2002. The human silent information
960 regulator (Sir)2 homologue hSIRT3 is a mitochondrial nicotinamide adenine
961 dinucleotide-dependent deacetylase. *J. Cell Biol.* 158:647–657.

962 Shahgaldi S, Kahmini FR. 2021. A comprehensive review of Sirtuins: With a major focus
963 on redox homeostasis and metabolism. *Life Sci.* 282:119803.

964 Sharma S, Ciufo S, Starchenko E, Darji D, Chlumsky L, Karsch-Mizrachi I, Schoch CL.
965 2019. The NCBI BioCollections Database. *Database* [Internet] 2019. Available
966 from: http://dx.doi.org/10.1093/database/baz057

967 Sheffield P, Garrard S, Derewenda Z. 1999. Overcoming expression and purification
968 problems of RhoGDI using a family of “parallel” expression vectors. *Protein Expr.*
969 *Purif.* 15:34–39.

970 Simó-Mirabet P, Bermejo-Nogales A, Calduch-Giner JA, Pérez-Sánchez J. 2017.
971 Tissue-specific gene expression and fasting regulation of sirtuin family in gilthead
972 sea bream (Sparus aurata). *Journal of Comparative Physiology B* [Internet]
973 187:153–163. Available from: http://dx.doi.org/10.1007/s00360-016-1014-0

974 Slade KM, Freggiaro S, Cottrell KA, Smith JJ, Wiley EA. 2011. Sirtuin-mediated nuclear
975 differentiation and programmed degradation in Tetrahymena. *BMC Cell Biol.* 12:40.

976 Smith JJ, Kuraku S, Holt C, Sauka-Spengler T, Jiang N, Campbell MS, Yandell MD,
977 Manousaki T, Meyer A, Bloom OE, et al. 2013. Sequencing of the sea lamprey
978 (Petromyzon marinus) genome provides insights into vertebrate evolution. *Nat.*
979 *Genet.* 45:415–421, 421e1–e2.

980 Somero GN. 2004. Adaptation of enzymes to temperature: searching for basic
981 "strategies." *Comp. Biochem. Physiol. B Biochem. Mol. Biol.* 139:321–333.

982 Stelzer G, Rosen N, Plaschkes I, Zimmerman S, Twik M, Fishilevich S, Stein TI, Nudel
983 R, Lieder I, Mazor Y, et al. 2016. The GeneCards Suite: From Gene Data Mining to
984 Disease Genome Sequence Analyses. *Curr. Protoc. Bioinformatics* 54:1.30.1–
985 1.30.33.

986 Tao R, Coleman MC, Pennington JD, Ozden O, Park S-H, Jiang H, Kim H-S, Flynn CR,
987 Hill S, Hayes McDonald W, et al. 2010. Sirt3-mediated deacetylation of
988 evolutionarily conserved lysine 122 regulates MnSOD activity in response to stress.
989 *Mol. Cell* 40:893–904.

990 Tatone C, Di Emidio G, Barbonetti A, Carta G, Luciano AM, Falone S, Amicarelli F.
991 2018. Sirtuins in gamete biology and reproductive physiology: emerging roles and
992 therapeutic potential in female and male infertility. *Hum. Reprod. Update* 24:267–
993 289.

994 Tenorio MJ, Ross BH, Luchsinger C, Rivera-Dictter A, Arriagada C, Acuña D, Aguilar M,
995 Cavieres V, Burgos PV, Ehrenfeld P, et al. 2016. Distinct Biochemical Pools of
996 Golgi Phosphoprotein 3 in the Human Breast Cancer Cell Lines MCF7 and MDA-
997 MB-231. *PLoS One* 11:e0154719.

998 Trifinopoulos J, Nguyen L-T, von Haeseler A, Minh BQ. 2016. W-IQ-TREE: a fast online
999 phylogenetic tool for maximum likelihood analysis. *Nucleic Acids Res.* 44:W232–
1000 W235.

1001 Tseng AHH, Shieh S-S, Wang DL. 2013. SIRT3 deacetylates FOXO3 to protect
1002 mitochondria against oxidative damage. *Free Radic. Biol. Med.* 63:222–234.

1003 Vassilopoulos A, Fritz KS, Petersen DR, Gius D. 2011. The human sirtuin family:
1004 evolutionary divergences and functions. *Hum. Genomics* 5:485–496.

1005 Vassilopoulos A, Pennington JD, Andresson T, Rees DM, Bosley AD, Fearnley IM, Ham
1006 A, Flynn CR, Hill S, Rose KL, et al. 2014. SIRT3 deacetylates ATP synthase F1
1007 complex proteins in response to nutrient- and exercise-induced stress. *Antioxid.*
1008 *Redox Signal.* 21:551–564.

1009 Vazquez BN, Vaquero A, Schindler K. 2020. Sirtuins in female meiosis and in
1010 reproductive longevity. *Mol. Reprod. Dev.* 87:1175–1187.

1011 Waterhouse A, Bertoni M, Bienert S, Studer G, Tauriello G, Gumienny R, Heer FT, de
1012 Beer TAP, Rempfer C, Bordoli L, et al. 2018. SWISS-MODEL: homology modelling
1013 of protein structures and complexes. *Nucleic Acids Res.* 46:W296–W303.

1014 Wichmann IA, Zavala K, Hoffmann FG, Vandewege MW, Corvalán AH, Amigo JD,
1015 Owen GI, Opazo JC. 2016. Evolutionary history of the reprimo tumor suppressor
1016 gene family in vertebrates with a description of a new reprimo gene lineage. *Gene*

1017 591:245–254.

1018 Wood JG, Rogina B, Lavu S, Howitz K, Helfand SL, Tatar M, Sinclair D. 2004. Sirtuin
1019 activators mimic caloric restriction and delay ageing in metazoans. *Nature*
1020 430:686–689.

1021 Yang L, Ma X, He Y, Yuan C, Chen Q, Li G, Chen X. 2017. Sirtuin 5: a review of
1022 structure, known inhibitors and clues for developing new inhibitors. *Sci. China Life*
1023 *Sci.* 60:249–256.

1024 Yates AD, Achuthan P, Akanni W, Allen J, Allen J, Alvarez-Jarreta J, Amode MR,
1025 Armean IM, Azov AG, Bennett R, et al. 2020. Ensembl 2020. *Nucleic Acids Res.*
1026 48:D682–D688.

1027 You W, Zheng W, Weiss S, Chua KF, Steegborn C. 2019. Structural basis for the
1028 activation and inhibition of Sirtuin 6 by quercetin and its derivatives. *Sci. Rep.*
1029 9:19176.

1030 Zhang J, Xiang H, Liu J, Chen Y, He R-R, Liu B. 2020. Mitochondrial Sirtuin 3: New
1031 emerging biological function and therapeutic target. *Theranostics* 10:8315–8342.

1032 Zhao E, Hou J, Ke X, Abbas MN, Kausar S, Zhang L, Cui H. 2019. The Roles of Sirtuin
1033 Family Proteins in Cancer Progression. *Cancers* [Internet] 11. Available from:
1034 http://dx.doi.org/10.3390/cancers11121949

1035 Zhao H-C, Ding T, Ren Y, Li T-J, Li R, Fan Y, Yan J, Zhao Y, Li M, Yu Y, et al. 2016.
1036 Role of Sirt3 in mitochondrial biogenesis and developmental competence of human
1037 in vitro matured oocytes. *Hum. Reprod.* 31:607–622.

1038